Author Manuscript Published OnlineFirst on December 15, 2021; DOI: 10.1158/0008-5472.CAN-21-2745
Author manuscripts have been peer reviewed and accepted for publication but have not yet been edited.

Integrated Metabolic Profiling and Transcriptional Analysis Reveals Therapeutic Modalities for Targeting Rapidly Proliferating Breast Cancers

Chengheng Liao[1,8], Cherise Ryan Glodowski[2,3,8], Cheng Fan[3], Juan Liu[4], Kevin R. Mott[3], Akash Kaushik[5], Hieu Vu[5], Jason W. Locasale[4], Samuel K. McBrayer[5], Ralph J. DeBerardinis[5,6], Charles M. Perou[2,3,7,*], and Qing Zhang[1,*]

[1] Department of Pathology, University of Texas Southwestern Medical Center, Dallas, TX 75390, USA

[2] Department of Pathology and Laboratory Medicine, University of North Carolina School of Medicine, Chapel Hill, NC 27599, USA

[3] Lineberger Comprehensive Cancer Center, University of North Carolina School of Medicine, Chapel Hill, NC 27599, USA

[4] Department of Pharmacology and Cancer Biology, Duke University School of Medicine, Durham, NC 27710, USA.

[5] Children's Medical Center Research Institute, University of Texas Southwestern Medical Center, 5323 Harry Hines Boulevard, Dallas, TX 75390, USA.

[6] Howard Hughes Medical Institute, University of Texas Southwestern Medical Center, 5323 Harry Hines Boulevard, Dallas, TX 75390, USA.

[7] Department of Genetics, University of North Carolina School of Medicine, Chapel Hill, NC 27599, USA

[8] These authors contributed equally

* Co-corresponding authors (Q.Z or C.P):

Running title: Metabolic profiling in breast cancer.

Downloaded from cancerres.aacrjournals.org on December 16, 2021. © 2021 American Association for Cancer Research.

Author Manuscript Published OnlineFirst on December 15, 2021; DOI: 10.1158/0008-5472.CAN-21-2745
Author manuscripts have been peer reviewed and accepted for publication but have not yet been edited.

Keywords: Breast cancer, Triple-negative breast cancer, Metabolic profiling, Targeted therapy, Chemotherapy

Financial support: This work was supported by Cancer Prevention and Research Institute of Texas (Q. Zhang, CPRIT, RR190058) and ACS Research Scholar Award (Q. Zhang, RSG-18-059-01-TBE), NCI Breast SPORE program (C.M. Perou, P50CA58223), National Cancer Institute (Q.Z, R01CA256833. C.M. Perou, R01CA148761) and BCRF (C.M. Perou).

Conflict of interest statement: Q.Z received consultation fee from Bristol Myers Squibb (BMS). C.M.P is an equity stock holder and consultant of BioClassifier LLC; C.M.P is also listed an inventor on patent applications on the Breast PAM50 Subtyping assay.

Corresponding authors

Qing Zhang, Ph.D, Email: Qing.Zhang@UTSouthwestern.edu

Department of Pathology
UT Southwestern Medical Center
5323 Harry Hines Blvd., NB7.208
Dallas, Texas 75390-9072
Tel: 214-645-4671
Fax: 214-648-1102

Charles Perou, Ph.D, Email: cperou@med.unc.edu

UNC Lineberger Comprehensive Cancer Center
Marsico Hall, 5th floor 5111, CB#7295, 125 Mason Farm Road
Chapel Hill, NC 27599
Tel: 919-843-5740

Downloaded from cancerres.aacrjournals.org on December 16, 2021. © 2021 American Association for Cancer Research.

Author Manuscript Published OnlineFirst on December 15, 2021; DOI: 10.1158/0008-5472.CAN-21-2745
Author manuscripts have been peer reviewed and accepted for publication but have not yet been edited.

Abstract

Metabolic dysregulation is a prominent feature in breast cancer, but it remains poorly characterized in patient tumors. In this study, untargeted metabolomics analysis of triple-negative breast cancer (TNBC) and estrogen receptor (ER)-positive breast cancer patient samples, as well as TNBC patient-derived xenografts (PDX), revealed two major metabolic groups independent of breast cancer histological subtypes: a "Nucleotide/Carbohydrate-Enriched" group and a "Lipid/Fatty Acid-Enriched" group. Cell lines grown in vivo more faithfully recapitulated the metabolic profiles of patient tumors compared to those grown in vitro. Integrated metabolic and gene expression analyses identified genes that strongly correlate with metabolic dysregulation and predict patient prognosis. As a proof-of-principle, targeting Nucleotide/Carbohydrate-Enriched TNBC cell lines or PDX xenografts with a pyrimidine biosynthesis inhibitor or a glutaminase inhibitor led to therapeutic efficacy. In multiple in vivo models of TNBC, treatment with the pyrimidine biosynthesis inhibitor conferred better therapeutic outcomes than chemotherapeutic agents. This study provides a metabolic stratification of breast tumor samples that can guide the selection of effective therapeutic strategies targeting breast cancer subsets. In addition, we have developed a public, interactive data visualization portal (http://brcametab.org) based on the data generated from this study to facilitate future research.

Significance

A multi-omics strategy that integrates metabolic and gene expression profiling in patient tumor samples and animal models identifies effective pharmacological approaches to target rapidly proliferating breast tumor subtypes.

Downloaded from cancerres.aacrjournals.org on December 16, 2021. © 2021 American Association for Cancer Research.

Author Manuscript Published OnlineFirst on December 15, 2021; DOI: 10.1158/0008-5472.CAN-21-2745
Author manuscripts have been peer reviewed and accepted for publication but have not yet been edited.

Introduction

Breast cancer is the most commonly diagnosed malignancy and 2nd most frequent cause of cancer-associated death for women worldwide (1). Triple-negative breast cancer (TNBC), which accounts 15-20% all breast cancers (2), is a clinically defined breast cancer subtype lacking estrogen and progesterone hormone receptor (ER and PR) expression and human epidermal growth factor receptor 2 (HER2) gene amplification (2). TNBC is featured by clinically aggressive and heterogeneous, highly metastatic, and shorter survival times compared to other subtypes such as ER^+ and $HER2^+$ breast cancers (2). The absence of a valuable therapeutic target in TNBC leaves the patients with limited treatment options, which is mostly focused upon canonical chemotherapy. Therefore, there is an urgent need to identify novel targets in TNBC.

Tumor cells often undergo metabolic alterations to fulfill the high demands of uncontrolled cell proliferation and tumorigenesis, which is a hallmark of cancer (3, 4). Therefore, tumor cell metabolism can be considered cancer's Achilles' heel and is a proven target of successful therapies (5-7). Cancer metabolic alterations include reprogramming of glycolysis, glutaminyl's, oxidative phosphorylation (OXPHOS), fatty acid metabolism, etc., which provide essential energy, biosynthesis intermediates, division and redox homeostasis for tumor growth (7). Therefore, a better understanding of breast tumor cell metabolism can potentially lead to novel therapeutic strategies through targeting specific metabolic pathways dysregulated in tumors while sparing the normal cells. Recently, several studies suggest that there is a unique metabolic dependence in some subsets of TNBCs, including TNBCs in patients undergoing chemotherapy or displaying PI3K/Akt hyper-activation (8-10). However, it remains

Downloaded from cancerres.aacrjournals.org on December 16, 2021. © 2021 American Association for Cancer Research.

Author Manuscript Published OnlineFirst on December 15, 2021; DOI: 10.1158/0008-5472.CAN-21-2745
Author manuscripts have been peer reviewed and accepted for publication but have not yet been edited.

unclear how we can potentially target the specific metabolic vulnerabilities in TNBC compared to other subtypes of breast cancer. In addition, given the well-known heterogeneity of TNBC, it remains unclear whether we can stratify TNBC patients according to their metabolic abnormalities and design rational metabolic therapeutic modalities against subsets of TNBC.

Our study comprehensively investigated the metabolic phenotypes, as well as gene expression phenotypes, of breast tumor patient samples, TNBC patient-derived xenografts (PDXs), and cell lines grown *in vitro* and *in vivo* from representative breast cancer subtypes including TNBC and ER^+ breast cancers. In this array of systematic analyses, we identified the specific metabolites that are enriched in ER^+ tumors and TNBCs. We also examined the correlation between metabolites and gene expression features. Lastly, we performed functional validation experiments by targeting the dysregulated metabolic pathways pharmacologically in multiple TNBC models.

Materials and Methods

Patient samples and cell lines

Breast cancer tumors and normal breast tissue samples were obtained from patients from the UNC Tissue Procurement Facility. Written informed consent was obtained from patients. Primary tumor and normal tissues were obtained, flash frozen, and then used for metabolite profiling and RNA extraction and sequencing. These tumor specimens were cut in half, with half used to make RNA and half used for metabolite extraction. These patient samples were de-identified and anonymized. An Institutional Review Board (IRB) exemption has been obtained in this study and thus this was considered non-Human Subjects Research. MDA-MB-231 and MCF-7 cells were

Downloaded from cancerres.aacrjournals.org on December 16, 2021. © 2021 American Association for Cancer Research.

Author Manuscript Published OnlineFirst on December 15, 2021; DOI: 10.1158/0008-5472.CAN-21-2745
Author manuscripts have been peer reviewed and accepted for publication but have not yet been edited.

cultured in Dulbecco's Modified Eagle's Medium (DMEM) (Gibco 11965118) supplemented with 10% fetal bovine serum (FBS) and 1% penicillin-streptomycin. T47D, HCC1428, HCC70, HCC1806, ZR-75-1, and MDA-MB-468 cells were cultured in 10% FBS, 1% penicillin-streptomycin RPMI 1640 (Gibco 11875093). All cell lines were obtained from ATCC. Cells were used for experiments within 10-20 passages from thawing. All cell lines were authenticated via short tandem repeat testing. Mycoplasma detection was routinely performed to ensure cells were not infected with mycoplasma by using MycoAlert Detection kit (Lonza, LT07-218).

Drugs

Brequinar (HY-108325) and CB-839 (Synonyms: Telaglenastat, HY-12248) were purchased from MedChem Express. Brequinar was dissolved in 10% DMSO and 90% sterilized corn oil. CB-839 drug was formulated in the special diet made by Research Diets Inc. which containing 1400 mg/kg diet dose of CB-839 drug. Paclitaxel and Carboplatin were purchased from Henry Schein Medical. anti-mouse PD-1 (BE0146) and rat IgG2a isotype control (BE0089) were purchased from Bio X Cell.

Metabolite extraction

The flash frozen patient tumors, normal breast tissues, PDX tumors, and cell line xenograft tumors were first cut in small pieces on dry ice, then 30 to 100 mg sections were weighed in a new 2 mL Eppendorf tube. 500 μL 80% (vol/vol) methanol (pre-cooled in −80 °C) was added to each tissue sample. The tissue chunk was further broken down on ice to form an even suspension by using a rotor-stator homogenizer (TissueRuptor, Qiagen). An additional 500 μL pre-cooled 80% methanol was added in each tube and vortexed rigorously for 1 min. After incubation on ice for an additional 10

Downloaded from cancerres.aacrjournals.org on December 16, 2021. © 2021 American Association for Cancer Research.

Author Manuscript Published OnlineFirst on December 15, 2021; DOI: 10.1158/0008-5472.CAN-21-2745
Author manuscripts have been peer reviewed and accepted for publication but have not yet been edited.

min, the tissue extract was centrifuged at 20,000 g at 4 °C for 15 min. The supernatant, normalized to the amount weighed of the samples, was transferred into clean Eppendorf tubes. For metabolite extraction from cell lines grown *in vitro*, cell lines were grown in 6-well plates for 2 days to 90% confluence. The culture medium was completely removed, cells were rinsed twice with 2 mL of cold normal saline solution to remove the medium residue completely. Cells were immediately placed on dry ice, followed by the addition of 1 mL 80% (vol/vol) methanol (pre-cooled in −80 °C) to each well. After incubation in −80 °C for 15 min, cells were scraped into 80% methanol on dry ice, transferred to Eppendorf tubes, and centrifuged at 20,000 g for 15 min at 4°C. The supernatant was normalized to cell number and transfer into Eppendorf tubes. Finally, the tubes were speed vacuum dried at room temperature then store dry pellet in -80 °C freezer for further LC-MS analysis.

Metabolomics/metabolite analysis

Metabolomics analysis was performed as previously described (11). Briefly, the dry pellets were reconstituted into 30 μL sample solvent (water:methanol:acetonitrile, 2:1:1, v/v) and 3 μL was further analyzed by liquid chromatography-mass spectrometry (LC-MS). Ultimate 3000 UHPLC (Dionex) was coupled to Q Exactive Plus-Mass spectrometer (QE-MS, Thermo Scientific) for metabolite profiling. A hydrophilic interaction chromatography method (HILIC) employing an Xbridge amide column (100 x 2.1 mm i.d., 3.5 μm; Waters) was used for polar metabolite separation. Detailed LC method was described previously (12) except that mobile phase A was replaced with water containing 5 mM ammonium acetate (pH 6.8). The QE-MS was equipped with a HESI probe with related parameters set as below: heater temperature, 120 °C; sheath

Downloaded from cancerres.aacrjournals.org on December 16, 2021. © 2021 American Association for Cancer Research.

Author Manuscript Published OnlineFirst on December 15, 2021; DOI: 10.1158/0008-5472.CAN-21-2745
Author manuscripts have been peer reviewed and accepted for publication but have not yet been edited.

gas, 30; auxiliary gas, 10; sweep gas, 3; spray voltage, 3.0 kV for the positive mode and 2.5 kV for the negative mode; capillary temperature, 320 °C; S-lens, 55; A scan range (m/z) of 70 to 900 was used in positive mode from 1.31 to 12.5 minutes. For negative mode, a scan range of 70 to 900 was used from 1.31 to 6.6 minutes and then 100 to 1,000 from 6.61 to 12.5 minutes; resolution: 70000; automated gain control (AGC), 3×10^6 ions. Customized mass calibration was performed before data acquisition. LC-MS peak extraction and integration were performed using commercially available software Sieve 2.2 (Thermo Scientific). The integrated peak area was used to represent the relative abundance of each metabolite in different samples. The missing values were handled as described in a previous study (12).

Metabolomics data analysis

The 40 patient and PDX samples were extracted, normalized by tissue weight used for metabolite extraction and measured by LC-MS at the same time. The metabolomics data was combined in some cases by removing any missing data and keep only the common metabolites that detected in all samples. The annotated metabolites from Kyoto Encyclopedia of Genes and Genomes (KEGG) Compound database (www.genome.jp/kegg) (13) and human metabolome database (HMDB; www.hmdb.ca) (14) were used for further analysis. The data matrix was then normalized in the following sequential steps: two-based log transformation, row median centering then followed by column standardization. All hierarchical clustering was performed using the normalized data by the Cluster 3.0 software and visualized by Java TreeView (1.1.6r4). Hierarchical clustering was performed using the following parameters: similarity measure: Euclidean distance: clustering algorithm: centroid linkage. Principal

Downloaded from cancerres.aacrjournals.org on December 16, 2021. © 2021 American Association for Cancer Research.

Author Manuscript Published OnlineFirst on December 15, 2021; DOI: 10.1158/0008-5472.CAN-21-2745
Author manuscripts have been peer reviewed and accepted for publication but have not yet been edited.

component analysis (PCA) and KEGG-based pathway enrichment analysis and pathway topology analysis was applied using the MetaboAnalyst 5.0 (https://www.metaboanalyst.ca/) (15).

Differential abundance (DA) score

The differential abundance (DA) score calculation was described in a previous study with some modifications (16). The DA score captures the tendency for a pathway to have increased levels of metabolites, relative to a control group. Briefly, the detected metabolites were first assigned to different metabolic pathway categories based on the KEGG pathways by MetaboAnalyst 5.0 software (15). Then a statistical analysis method (SAM analysis has been used in this study; see Statistical Analysis section for detail) was applied to determine which metabolites are significantly increased or decreased in abundance in a pathway between different sample groups. Then, after determining the significant increased/decreased metabolites, the DA score was calculated based on the following formular:

DA score = (number of metabolites increased - number of metabolites decreased) / number of measured metabolites in a pathway

Thus, the DA score varies from -1 to 1. A score of 1 indicates that all metabolites in a pathway increased in abundance, while a score of -1 indicates that all metabolites decreased. Consider a limited detection capability by LC-MS but important role of metabolites for some pathways. Pathways with no less than 2 detected metabolites were used for DA score calculation.

RNA sequencing

Downloaded from cancerres.aacrjournals.org on December 16, 2021. © 2021 American Association for Cancer Research.

Author Manuscript Published OnlineFirst on December 15, 2021; DOI: 10.1158/0008-5472.CAN-21-2745
Author manuscripts have been peer reviewed and accepted for publication but have not yet been edited.

Total RNA was isolated from tumors, normal breast tissues, and PDXs using the RNeasy Plus Mini kit (Qiagen), with additional on-column DNase treatment to eliminate traces of genomic DNA. mRNAseq libraries were made from total RNA using the Illumina TruSeq mRNA sample preparation kit and sequenced on an Illumina HiSeq 2500 using a 2x50bp configuration. Purity-filtered reads were aligned to the human reference GRCh38/hg38 genome using Spliced Transcripts Aligned to a Reference (STAR) version 2.4.2a1. Transcript (GENCODE v22) abundance estimates were generated by Salmon version 0.6.02 in '-quant' mode, based on the STAR alignments. Raw read counts for all RNAseq samples were normalized to a fixed upper quartile3. RNAseq normalized gene counts were then log2 transformed (zeros were unchanged), and genes were filtered for those expressed in 70% of samples.

PAM50 subtyping

To determine the intrinsic subtypes, we used clinical biomarker statuses and RNAseq gene expression data from 40 samples that included 9 normal breast tissues, 9 ER^+ breast tumor samples, 15 TNBC (ER^-/$HER2^-$/PR^-) breast tumor samples, and 7 individual tumors from 2 TNBC patient-derived xenografts (WHIM2 and WHIM30). To obtain the subtype-related biomarkers from our mRNAseq gene expression data, we first used an ER/HER2 subgroup-specific gene normalization method, using the IHC status assigned to each sample. This normalization was done prior to applying the PAM50 predictor to correct differences in the biological composition and any technical bias between the gene expression of our 40 study samples derived from RNAseq and the Agilent Human Microarrays used to create the original PAM50 UNC232 training set (17). After labeling samples with their ER/HER2 status, we then extracted the ER/HER2

Downloaded from cancerres.aacrjournals.org on December 16, 2021. © 2021 American Association for Cancer Research.

Author Manuscript Published OnlineFirst on December 15, 2021; DOI: 10.1158/0008-5472.CAN-21-2745
Author manuscripts have been peer reviewed and accepted for publication but have not yet been edited.

subgroup-specific percentile centering genes, with the percentile determined from the subgroup of the clinicopathological classifications (See detailed method description in supplemental methods) (18). We then normalized the expression values of the PAM50 genes present in our 40 samples. After gene normalization, we applied the PAM50 predictor (17). This calculated the correlation coefficient to the PAM50 centroids, and allowed us to assign following intrinsic molecular subtypes to each sample: Basal-like, HER2-Enriched, Luminal A, Luminal B, and Normal-like signatures.

Proliferation signature and calculation

We determined proliferation scores for each of our 40 tumor samples using the Zhao et al (2015) PAM50 subtyping method (18), which outputs a proliferation score for each sample by utilizes a proliferation signature is based on the average expression of 11 key proliferation genes linked to cell cycle progression described by Nielson et al (2010) (19). This proliferation signature is known to provide robust, prognostic information for disease-free survival (Nielson et al., 2010). To replicate this proliferation score on our Brauer et al (2013) validation test set, the expression values for the 10/11 expressed proliferation score genes (*CDC20, KNTC2, MKI67, PTTG1, RRM2, TYMS, UBE2C, BIRC5, CCNB1, CDCA1*) were median-averaged and used as the proliferation scores for correlating metabolite signatures with proliferation potential.

***In vivo* isotope tracing**

Six-week old female NOD SCID Gamma mice (NSG, Jackson lab) were injected with 1×10^6 viable HCC1806 cells orthotopically into the mammary fat pad. Upon tumors establishment (~1000 mm^3), mice were treated with CB-839 for 3 days or Brequinar for 3 doses of injections before the tracing experiment. The *in vivo* isotope tracing

Downloaded from cancerres.aacrjournals.org on December 16, 2021. © 2021 American Association for Cancer Research.

Author Manuscript Published OnlineFirst on December 15, 2021; DOI: 10.1158/0008-5472.CAN-21-2745
Author manuscripts have been peer reviewed and accepted for publication but have not yet been edited.

experiment was described previously (20). Briefly, $^{13}C_5$- or $^{15}N_2$-glutamine (Cambridge Isotope Laboratories) were dissolved in sterilized saline. 200uL of 0.2M $^{13}C_5$- or $^{15}N_2$-glutamine solution were injected 3 times with 15-minute interval into the tail vein under anesthesia. Mice were euthanized via cervical dislocation at 45 min after first injection. Tumor tissue was rapidly harvested and snap frozen in liquid nitrogen and stored at -80℃ prior to metabolite extraction.

Animal studies

All orthotopic tumor xenograft animal experiments were in compliance with (21) and were approved by the University of Texas Southwestern Medical Center Animal Care and Use Committee, and all TNBC PDX and Trp53-null transplant model experiments were performed in accordance with approved University of North Carolina (UNC) Institutional Animal Care and Use Committee protocols.

Orthotopic tumor xenograft

Six-week old female NOD SCID Gamma mice (NSG, Jackson lab) were used for xenograft studies. Approximately 1×10^6 viable HCC1806 or MDA-MB-468 cells were resuspended a mixture of 50 μL Matrigel (Corning, 354234) and 50 μL FBS-free growth medium and injected orthotopically into the mammary fat pad of each mouse. Treatment was started when HCC1806 tumors reached the volume of approximately 150 mm^3 and MDA-MB-468 tumors reached the volume of approximately 50 mm^3, considering tumorigenesis ability of each cell line.

TNBC PDX and Trp53-null transplant model

Downloaded from cancerres.aacrjournals.org on December 16, 2021. © 2021 American Association for Cancer Research.

Author Manuscript Published OnlineFirst on December 15, 2021; DOI: 10.1158/0008-5472.CAN-21-2745
Author manuscripts have been peer reviewed and accepted for publication but have not yet been edited.

The TNBC PDX model for treatments used in this study was the WHIM2, obtained from the Washington University in St Louis MO. The NSG mice (NOD SCID GAMMA mice) were obtained from the Jackson Laboratory or supplied in-house by the UNC Animal Services Core (ASC). The Trp53-null transplant model has phenotypically and genomically diverse tumors that can be classified into three major subtypes/classes based on gene expression profiles: p53null Basal, Claudin-low and p53null-Luminal (22). The five validated Balb/C Trp53-null serial transplant models used in this study were 2336R, 9263-3, 2224L, 2225L, and T-11. The Balb/C female mice used were obtained from the Jackson Laboratory.

Tumor transplantation for TNBC PDX and Trp53-null transplant model

Tumors were digested with the Miltenyi tumor dissociation kit to establish cell aggregate suspensions. Cell aggregates were subsequently washed in Hank's Balanced Salt solution containing 2% FBS (HF Media) and resuspended in HF media with 50% Matrigel prior to transplant into cohort mice. Mice were briefly anesthetized with 2% isoflurane and tumor cells were injected into the inguinal mammary fat pad of Balb/C mice. Mice were followed 2-3 times weekly with caliper measurement for the establishment of tumors and upon reaching a diameter of 0.5 cm were randomly assigned into either treatment or control groups.

Treatment with drugs

Prior to treatment, the tumor-bearing mouse cohorts for the orthotopic xenograft, TNBC PDX, or Trp53-null murine tumors were divided into different groups by randomization. Tumor-bearing mice in the treatment group were continuously administered a specially formulated chow containing 1400 mg/kg diet dose of CB-839 or

Downloaded from cancerres.aacrjournals.org on December 16, 2021. © 2021 American Association for Cancer Research.

Author Manuscript Published OnlineFirst on December 15, 2021; DOI: 10.1158/0008-5472.CAN-21-2745
Author manuscripts have been peer reviewed and accepted for publication but have not yet been edited.

an intraperitoneal (I.P.) injection of 20 mg/kg Brequinar every 3 or 4 days, or a combination of both. Mice in the Carbo/Tax treatment group were administered I.P. injections of Paclitaxel (10mg/kg dose) and Carboplatin (50 mg/kg dose) once per week. For 4T1 model, 5×10^5 cells were orthotropic injected into Balb/C mice. Mice received biweekly I.P. injections of 0.2 mg of PD-1 mAb or IgG2a control mAb in 100 μL of PBS from day 8 for a total of 4 doses. Brequinar or combination treatment were started at the same time. Tumor size was measured by caliper and body weight was recorded every 3 or 4 days. Tumor volumes were calculated with the formula: volume=$(L\times W^2)/2$, where L is the tumor length and W is the tumor width measured in millimeters. All mice were observed for overall condition and weighed weekly. For the survival study, mice were sacrificed when tumor reached 2 cm in any dimension.

Statistical analysis

A statistical method specialized for multi-testing, SAM (Significance Analysis of Microarrays) (23) was applied to identify differential abundant metabolites or differentially expressed genes in the patient samples. Specifically, we used SAM to examine the correlation between abundance of each metabolite compounds or mRNA expression of each genes between different sample groups based on the unsupervised clustering. For all SAM analyses, distribution-independent ranking tests (based on the Wilcoxon test) and the sample-wise permutation (default by the samr package) were used to ascertain significance (false discovery rate, FDR<0.05). The SAM analysis gives a list of significantly upregulated (positive log fold change) or downregulated (negative log fold change) features between different sample groups with a q-value<0.05 were considered statistically significance.

Downloaded from cancerres.aacrjournals.org on December 16, 2021. © 2021 American Association for Cancer Research.

Author Manuscript Published OnlineFirst on December 15, 2021; DOI: 10.1158/0008-5472.CAN-21-2745
Author manuscripts have been peer reviewed and accepted for publication but have not yet been edited.

All other statistical analysis was conducted using Prism 8.0 (GraphPad Software). All graphs depict mean ± SEM unless otherwise indicated. Statistical significances are denoted as not significant (ns; P>0.05), *P<0.05, **P<0.01, ***P<0.001, ****P<0.0001. The numbers of experiments are noted in figure legends. To assess the statistical significance of single metabolites between two groups, we used unpaired two-tail student's *t*-test. For animal experiments comparing more than two conditions, differences were tested by a one-way ANOVA followed by Dunnett's or Tukey's multiple comparison tests.

Data availability

The FASTQ files from RNAseq data and the star-salmon upper quartile normalized gene expression matrix are being deposited into the dbGAP (dbGaP Study Accession: phs002396.v1.p1) and GEO database (GEO Accession: GSE173991). The full set of metabolomics data can be accessed from the Supplementary Tables S2 and S3, or from the corresponding authors upon request.

Results

Metabolic profiling of patient breast cancer tumors and TNBC PDXs

To examine the metabolic profiles in TNBC and ER^+ breast cancer, we obtained 15 TNBC and 9 ER^+ flash frozen breast tumor samples; we also collected 7 flash frozen tumor samples from 2 TNBC PDX models (WHIM2 and WHIM30) grown in NOD Scid Gamma-deficient (NSG) mice (24) (Supplementary Table S1). We first extracted polar metabolites from these tumors followed by untargeted metabolomics analysis by liquid chromatography, high-resolution mass spectrometry (LC-MS) (Fig. 1A). A total of 301

Downloaded from cancerres.aacrjournals.org on December 16, 2021. © 2021 American Association for Cancer Research.

Author Manuscript Published OnlineFirst on December 15, 2021; DOI: 10.1158/0008-5472.CAN-21-2745
Author manuscripts have been peer reviewed and accepted for publication but have not yet been edited.

metabolites were detected in all 31 tumor samples with 263 well annotated by the Kyoto Encyclopedia of Genes and Genomes (KEGG) database (13) or the Human Metabolome Database (HMDB) (14) (Fig. 1B). Inquiring whether the global metabolic profiling could reveal differences in breast cancer subsets, we performed an unsupervised hierarchical clustering using the 263 annotated metabolites data from the 31 tumor samples (Fig. 1C; Supplementary Table S2). The cluster divided these patients into two distinctive metabolic clusters (Fig. 1C). Intriguingly, 7/15 TNBC tumors clustered with all of ER^+ breast tumors (Cluster 1) while all TNBC PDXs tumors grouped with 8/15 TNBC tumor samples (Cluster 2). The clustering pattern suggests metabolic variances among the TNBC tumors in terms of metabolite abundance. We also performed mRNA sequencing (mRNAseq) on all tumor samples and applied PAM50 subtyping based on gene expression to further interrogate the tumor molecular features (17). As expected, all TNBC PDXs and most TNBC tumors were basal-like breast cancer (9 out of 15), and most basal-like TNBCs (i.e., 6/9), together with the 7 basal-like PDXs, were present in the Cluster 2 (Fig. 1C), while all of the ER^+ and some of TNBC from Cluster 1 were luminal or normal-like subtype by the PAM50 analysis (Fig. 1C). We then performed a supervised statistical analysis (SAM (Significance Analysis of Microarrays), see Methods for details) to the metabolite data to identify the significantly altered metabolites between the two metabolic clusters (Supplementary Fig. S1A). Among the 263 annotated metabolites, 93 were significantly higher in Cluster 1 (35.3%; $q<0.05$, SAM), and 90 were significantly higher in Cluster 2 (34.2%; $q<0.05$, SAM) (Fig. 1D; Fig. S1, B and C).

Downloaded from cancerres.aacrjournals.org on December 16, 2021. © 2021 American Association for Cancer Research.

Author Manuscript Published OnlineFirst on December 15, 2021; DOI: 10.1158/0008-5472.CAN-21-2745
Author manuscripts have been peer reviewed and accepted for publication but have not yet been edited.

To investigate the metabolic alterations in the breast cancer patient tumors and PDXs stratified by the metabolic clusters, we performed a KEGG pathway-based differential abundance (DA, see Methods for details) analysis (16) using the metabolites significantly varied between Cluster 1 and 2 tumors. The DA analysis captured 49 metabolic pathways as being differentially abundant with a broad metabolic pathway category (Fig. 1E). Interestingly, most of the pathways elevated in the Cluster 1 tumors were lipid/fatty acid metabolism and some amino acid metabolism pathways such as glycine, serine and threonine metabolism, whereas pathways elevated in the Cluster 2 tumors were significantly enriched with pyrimidine and purine metabolism, energy production and carbohydrate metabolism (Fig. 1E). We also conducted integrated pathway enrichment and topology analysis (PA) by MetaboAnalyst (15), which considered the metabolite impact in each pathway and found some common pathways enriched from both DA and PA analyses (Supplementary Fig. S2, A and B). These pathway-based analyses were further illustrated by the differential abundance of individual key metabolites for each pathway category in these two clusters (Fig. 1C, F-I; Supplementary Fig. S2, C-F). Given the overall enrichment pattern for each cluster (Fig. 1C, F-H), we annotated “Lipid/Fatty Acid-Enriched” for Cluster 1 and “Nucleotide/Carbohydrate-Enriched” for Cluster 2 to highlight the metabolic features in these groups of patient tumors and PDXs. We also obtained 9 flash frozen normal breast tissues and performed metabolic profiling (Supplementary Fig. S3A) and found that these normal breast tissues clustered together with ER^+ breast tumor samples (Cluster 1) and did not change the overall distribution of the tumor sample clustering pattern or pathway enrichment in two clusters (Fig. S3, B-D). Taken together, our

Downloaded from cancerres.aacrjournals.org on December 16, 2021. © 2021 American Association for Cancer Research.

Author Manuscript Published OnlineFirst on December 15, 2021; DOI: 10.1158/0008-5472.CAN-21-2745
Author manuscripts have been peer reviewed and accepted for publication but have not yet been edited.

metabolic profiling in breast cancer patient tumors clearly classifies a subset of tumors in the Nucleotide/Carbohydrate-Enriched cluster enriched for basal-like/TNBC patient tumors and distinct from the Lipid/Fatty Acid-Enriched cluster that contained the other subtypes of breast cancers (and true normal).

Distinctive metabolism of breast cancer cell lines grown *in vivo* versus *in vitro*

Next, we asked whether the metabolic alteration observed in breast cancer patients was represented in cell lines in a subtype-specific and growth-context manner. To this end, we used representative breast cancer cell lines from 4 ER^+ (MCF-7, T47D, ZR-75-1 and HCC1428) and 4 TNBC (MDA-MB-231, MDA-MB-468, HCC70 and HCC1806). These cell lines were either implanted orthotopically in NSG mice (*in vivo* growth, n=3 mice/line) as described previously (25, 26) or cultured in parallel in petri dishes (*in vitro* growth, n=2 biological duplicates/line). When cell derived xenograft tumors reached a common size (~0.5 cm in diameter), tumors were harvested and underwent untargeted metabolomics analysis as described above (Fig. 2A; Supplementary Table S3). It is known that there are metabolic differences for cell lines grown *in vivo* versus *in vitro* (27). Therefore, we first examined the data with principal component analysis (PCA) which clearly separated the samples by the growth condition (Fig. 2B). Unsupervised hierarchical clustering further showed distinctive metabolic profiles between the cell lines grown in *in vitro* versus *in vivo* (Fig. 2C), regardless of subtypes of these cells (Supplementary Fig. S4, A and B). By comparing the metabolic pathway in these two cell growth conditions, metabolites significantly accumulated *in vitro* were enriched in several metabolic pathways, including amino acid metabolism, TCA cycle, and glycolysis/gluconeogenesis (Fig. 2D). Conversely, metabolic pathways enriched *in vivo*

Downloaded from cancerres.aacrjournals.org on December 16, 2021. © 2021 American Association for Cancer Research.

Author Manuscript Published OnlineFirst on December 15, 2021; DOI: 10.1158/0008-5472.CAN-21-2745
Author manuscripts have been peer reviewed and accepted for publication but have not yet been edited.

included nucleotide metabolism and some fatty acid metabolism (Fig. 2E). Further examination of representative metabolites revealed that glucose, pyruvate, 2-oxoglutarate, succinate, glutamine, and other amino acids were strongly enriched in cells grown *in vitro* (Fig. 2F) versus many pyrimidine and purine nucleotides were significantly higher in cells grown *in vivo* (Fig. 2G). This is expected given that most of these components (such as glucose, glutamine, pyruvate and amino acids) are abundant in the typical cell growth media and readily utilized by cells in the *in vitro* growth. We also performed analysis to compare *in vivo* versus *in vitro* within each breast cancer cell subtype and found very similar pathway enrichment results (Supplementary Fig. S4, C-F). These findings suggested that *in vitro* growth dramatically changed the metabolism compared to the *in vivo* growth in these breast cancer cells, irrespective of the subtype.

Metabolic profiling of cell line xenograft grown *in vivo* reveals similar metabolite enrichment as in patients

Next, we combined all the metabolomics data from the patient, PDX, and *in vitro* and *in vivo* cell lines to examine the metabolic profile. Overall, global unsupervised clustering of all samples suggests that the metabolism in cell lines grown *in vivo* and PDX tumors is more representative of breast tumors from patients (Fig. 3A). Therefore, we focused our analyses on the data of cell lines grown *in vivo*. We performed supervised comparison between the ER^+ and TNBC cell lines that revealed 43 and 45 differential abundant metabolites enriched in ER^+ and TNBC cells, respectively (Fig. 3B). PCA and hierarchical clustering analyses by these metabolites suggested two distinct groups between the ER^+ and TNBC *in vivo* cells (Fig. 3, C and D). Pathway analysis for

Downloaded from cancerres.aacrjournals.org on December 16, 2021. © 2021 American Association for Cancer Research.

Author Manuscript Published OnlineFirst on December 15, 2021; DOI: 10.1158/0008-5472.CAN-21-2745
Author manuscripts have been peer reviewed and accepted for publication but have not yet been edited.

each cell line subtype did not fully recapitulate the metabolic pathway enrichment results from patient tumors (Supplementary Fig. S5, A and B), which is possibly due to the relatively fewer metabolites significantly altered between the ER^+ and TNBC cells, and/or an overall highly proliferative character for these cancer cell lines grown *in vivo*. However, the abundance of some metabolites revealed high similarity between the ER^+ and TNBC subtypes, as we observed in the metabolic clusters from patient tumors (Fig. 3, E and F; Supplementary Fig. S5, C-E). These results suggest that pathways such as glucose, glutamine, and lipid/fatty acid metabolism were faithfully altered between the ER^+ and TNBC subtypes of breast cancer patients and cell lines grown *in vivo*. Therefore, the cell line *in vivo* model partially mimics the metabolism seen in actual tumor specimens.

Integrated analysis of patient metabolomics and transcriptomics data reveals valuable metabolite and gene signatures

Unique gene expression patterns, including PAM50 subtype and proliferation signatures, show prognostic value for breast cancer patients (17, 19). To rigorously evaluate possible relationships between metabolite and gene expression profiles (Fig. 4A), we first calculated median values of the Lipid/Fatty Acid-Enriched metabolite signature from Cluster 1 (n=93, Supplementary Fig. S1B) and Nucleotide/Carbohydrate-Enriched metabolite signature from Cluster 2 (n=90, Supplementary Fig. S1C) for each of the patient samples, and then compared these values according to their PAM50 subtype. For our data set of 31 tumor and 9 normal breast tissue samples, the Lipid/Fatty Acid-Enriched feature was higher in Luminal A and B samples compared with the basal-like samples, and was especially high in normal-like and true normal

Downloaded from cancerres.aacrjournals.org on December 16, 2021. © 2021 American Association for Cancer Research.

Author Manuscript Published OnlineFirst on December 15, 2021; DOI: 10.1158/0008-5472.CAN-21-2745
Author manuscripts have been peer reviewed and accepted for publication but have not yet been edited.

breast samples (Fig. 4B). Conversely, the Nucleotide/Carbohydrate-Enriched feature displayed significantly higher values in basal-like subtype tumors (Fig. 4B). Noted that there are 4 TNBC tumors in Cluster 1 with normal-like PAM50 subtype (Fig. 1C) whereas with a Lipid/Fatty Acid-Enriched metabolite profile, further suggesting the potential of using these metabolite signatures to stratify TNBC patients. Given the known association between PAM50 subtypes and proliferation rates (19), we next split these samples into tertiles (high, medium, and low) based on the median values of the two metabolite signatures, then plotted gene expression-based proliferation signature values (Fig. 4C). This analysis showed that a high Nucleotide/Carbohydrate-Enriched metabolite profile was significantly associated with high proliferation signature values, while the Lipid/Fatty Acid-Enriched metabolite profile correlated with low proliferation potential. To validate the metabolomic and genomic PAM50 profile relationships, we used genomic and metabolomics data from 32 human breast tumor and 6 normal breast tissue samples from a previous study by Brauer et al. (28) as a validation data set. We used the previously published PAM50 subtype classifications (28) and determined proliferation scores as well as metabolite scores with two clusters as described in the methods. Of the metabolite signatures from our study, 34 out of the 90 metabolites for the Nucleotide/Carbohydrate-Enriched metabolite signature and 22 out of 93 metabolites for the Lipid/Fatty Acid-Enriched metabolite signature were present in the validation data set. Using all 32 tumor and 6 normal samples (n=38), the Nucleotide/Carbohydrate-Enriched metabolite signature showed statistically significant differences by expression subtype ($p<0.01$) and was high in the basal-like tumors in this validation set, which is consistent with our current results (Supplementary Fig. S6A).

Downloaded from cancerres.aacrjournals.org on December 16, 2021. © 2021 American Association for Cancer Research.

Author Manuscript Published OnlineFirst on December 15, 2021; DOI: 10.1158/0008-5472.CAN-21-2745
Author manuscripts have been peer reviewed and accepted for publication but have not yet been edited.

However, the Lipid/Fatty Acid-Enriched signature did not show statistically significant differences in PAM50 subtypes (Supplementary Fig. S6A), possibly reflecting the small numbers matched metabolites in this validation set (22/93). We further split the 32 tumor samples into tertiles based on the median values of the Nucleotide/Carbohydrate-Enriched signature and proliferation score, which again showed higher values in highly proliferating tumors (Supplementary Fig. S6B), thus validating the predictive value of these metabolite signatures on a second specimen test set.

To identify genes that correlate with the metabolite signatures, we performed a supervised gene expression analysis based on the metabolic clustering (Fig. 4, A and D). Supervised analysis of gene expression by SAM based on the two metabolic clusters each gave rise to distinctive gene expression profiles and groups of differentially expressed (DE) genes ($q<0.05$, SAM) (Fig. 4D; Supplementary Fig. S6C). We herein define these genes as “Lipid/Fatty Acid-Enriched” or “Nucleotide/Carbohydrate-Enriched” associated gene signatures. For the Nucleotide/Carbohydrate-Enriched genes from Cluster 2, this analysis gave 2908 DE genes; when examing the top 200 DE genes, these genes were homogenously and highly expressed in Cluster 2 versus Cluster 1 tumors (Supplementary Fig. S6D). Gene ontology (GO) analysis using these top 200 DE genes, suggested they correlated strongly with biological processes including cell division, DNA replication, cell cycle, and cell proliferation (Fig. 4E). Importantly, when analyzed using the 1100 patients in the TCGA Breast Cancer data set (29), this top 200 gene mRNA profile correlated with multiple previously defined proliferation profiles, including the aforementioned PAM50 proliferation signature used in Fig. 4C and Supplementary Fig. S6B (Pearson correlation

Downloaded from cancerres.aacrjournals.org on December 16, 2021. © 2021 American Association for Cancer Research.

Author Manuscript Published OnlineFirst on December 15, 2021; DOI: 10.1158/0008-5472.CAN-21-2745
Author manuscripts have been peer reviewed and accepted for publication but have not yet been edited.

0.93). Next, we performed a similar analysis using the Lipid/Fatty Acid-Enriched metabolite profile and identified 6224 DE genes as being associated with this feature (q<0.05, SAM). Examining the Lipid/Fatty Acid-Enriched metabolite profile associated top 200 genes (Supplementary Fig. S6E) by GO analysis revealed that they were involved in angiogenesis, cellular response to hormone stimulus, and response to progesterone (Fig. 4F). These represent some of the canonical pathways generally enriched in the luminal breast cancers (30). To examine whether the metabolic clusters are also associated with immune-related signatures, we ran ANOVAs of published immune modules for our patient tumor training set (n=24) for each metabolite-determined cluster (Fig. 1C). We tested multiple immune-related signatures, including CIBERSORT_T_cells_CD8 (31), Bcell_Tcell_Cooperation (32), and single gene CD274/PD-L1. While our TNBC Metabolite-HIGH signature showed significant variance between two metabolite-detmined clusters as is expected (p<0.0001) (Supplementary Fig. S7A), none of the major immune signatures showed any significant variance between these two groups (Supplementary Fig. S7, B-D).

To determine whether these 200 gene signatures predict patient prognosis in breast cancer, we extracted gene expression data from the METABRIC (33) (n=1992), Harrell 2011 (34) (n=855), and SCAN-B data sets (35) (n=2969), then calculated the median expression of the Nucleotide/Carbohydrate-Enriched 200 DE genes followed by Kaplan-Meier (K-M) survival analysis according to tertiles of expression (Fig. 4G). High expression of these 200 genes strongly correlated with worse prognosis, which is expected given their high accordance to known proliferation signatures and the strong, known prognostic value of proliferation features in breast cancer (19, 36). Interestingly,

Downloaded from cancerres.aacrjournals.org on December 16, 2021. © 2021 American Association for Cancer Research.

Author Manuscript Published OnlineFirst on December 15, 2021; DOI: 10.1158/0008-5472.CAN-21-2745
Author manuscripts have been peer reviewed and accepted for publication but have not yet been edited.

survival analysis using the Lipid/Fatty Acid-Enriched 200 DE genes, we found that high expression of these genes predicted better prognosis in these datasets (Fig. 4H).

Pyrimidine metabolism and glutaminolysis pathways are elevated in TNBC

We further probed the relationships between gene expression and metabolite levels using the identified DE genes within each metabolic clusters (Fig. 4D) and performed metabolic focused gene set-based pathway analysis by the DAVID bioinformatics tools (37). Notably, pyrimidine and purine metabolism, carbon metabolism, and the energy production related pathways were highly enriched in Cluster 2 while many lipid/fatty acid metabolism related pathways were enriched in Cluster 1, suggesting the metabolic gene expression is associated with the metabolite abundance in the patient samples. This finding was further demonstrated by the joint-pathway analysis function from MetaboAnalyst using the significantly accumulated metabolites and upregulated DE genes from each cluster (Supplementary Fig. S8, A and B). Among these analyses, we found that the pyrimidine metabolism was the top pathway and its related metabolic genes were upregulated in Cluster 2 TNBC tumors (Fig. 5, B-D; Supplementary Fig. S8B). It is worth noting that pyrimidine biosynthesis was previously reported to be upregulated in response to chemotherapy exposure in TNBC (9). We also noticed that in all cases of metabolite analyses, TNBC patient tumors in Cluster 2, PDXs, and TNBC cell lines grown *in vivo* had marked high levels of glutamate and low levels of glutamine (Fig. 1I and 3E). Some of the key glutamine metabolism and transport enzymes gene expression such as the glutaminase (*GLS*) was upregulated in the Cluster 2 TNBC tumors (Fig. 5, C-E), suggesting the TNBC tumors maintains high level of glutamine metabolism compared to ER^+ breast tumors. In addition, PTEN mutant TNBC cells were

Downloaded from cancerres.aacrjournals.org on December 16, 2021. © 2021 American Association for Cancer Research.

Author Manuscript Published OnlineFirst on December 15, 2021; DOI: 10.1158/0008-5472.CAN-21-2745
Author manuscripts have been peer reviewed and accepted for publication but have not yet been edited.

dependent on glutamine flux through the *de novo* pyrimidine synthesis pathway, which rendered these cells to be sensitive to DHODH inhibitor treatment (10). Indeed, our steady-state metabolite profiling in patient tumors suggested that Cluster 2 TNBC tumors maintained high levels of glutaminolysis state with high levels of TCA cycle intermediates, glutamate and other downstream metabolites including arginine, proline, reduced glutathione (GSH), and high levels of *de novo* pyrimidine biosynthesis intermediates, concomitant with low level of glutamine and aspartate in these tumors (Fig. 5F). By examing the relative ratio both in the patient tumors and cell lines grown *in vivo*, we showed higher levels of glutamate/glutamine (Fig. 5G), carbamoyl-aspartate/glutamine (Fig. 5H), and carbamoyl-aspartate/aspartate (Fig. 5I) in TNBC versus ER^+ breast cancer. These results suggest that the glutaminolysis and pyrimidine metabolism pathways are elevated in TNBC.

It is worth noting that glutamine-dependent catabolism feeds multiple biosynthetic pathways including nucleotides, lipids, TCA cycle, and others (38), and a recent study showed that glutamine metabolism was the major energy and nucleotide resources for cancer cells (39). To confirm that the glutaminolysis and pyrimidine metabolism are directly from the glutamine metabolism in TNBC, we performed *in vivo* isotope tracing experiment in a basal-like TNBC cell xenograft model. Bolus intravenous injection of $^{13}C_5$-glutamine through tail vein within 45 mins (20) led to a rapid glutamine pool labeling in the HCC1806 xenograft tumors (Fig. 5J). Notably, bolus infusion also revealed significant pool labeling of glutamate and aspartate but not other amino acids (Fig. 5J). We also noticed high levels of labelled TCA cycle intermediates such as succinate, fumarate, and citrate, but minimal labeling of GSH or GSSG (Fig. 5K).

Downloaded from cancerres.aacrjournals.org on December 16, 2021. © 2021 American Association for Cancer Research.

Author Manuscript Published OnlineFirst on December 15, 2021; DOI: 10.1158/0008-5472.CAN-21-2745
Author manuscripts have been peer reviewed and accepted for publication but have not yet been edited.

Intriguingly, some of the pyrimidine nucleotides and nucleotide sugars were also labelled in the carbon backbone through $^{13}C_5$-glutamine infusion, which may largely be due to the indirect fueling from labelled aspartate (Fig. 5L). To confirm the fueling from glutamine to *de novo* pyrimidine biosynthesis, we also bolus infused the HCC1806 xenograft with $^{15}N_2$-glutamine and observed significant labelling of the pyrimidine nucleotides in 45 mins (Fig. 5M). Altogether, these results demonstrate that glutamine catabolism-based pyrimidine metabolism and glutaminolysis pathways are highly required in TNBC.

Combinatorial targeting of pyrimidine and glutamine metabolism in TNBC models

Next, we sought to explore therapeutic opportunities by targeting the pyrimidine and/or glutamine metabolism in TNBC models. To target glutamine metabolism, we used the drug CB-839 to inhibit the GLS enzyme, and to target pyrimidine metabolism, we used the drug Brequinar to inhibit DHODH, the enzyme that converts dihydroorotate to orotate (Fig. 6A). To understand how glutamine metabolism changes in TNBC cells upon CB-839 treatment, we bolus-infused the HCC1806 tumors with $^{13}C_5$-glutamine with or without CB-839 treatment. We found significant decrease of the labeled glutamate (Fig. 6B) and its downstream metabolites related to glutamate metabolism (Fig. 5F), including aspartate, proline, and arginine biosynthesis intermediates (Fig. 6B), as well as TCA cycle intermediates and glutathione (Fig. 6C) by CB-839 treatment. Similarly, we bolus-infused the HCC1806 tumors with $^{15}N_2$-glutamine with or without Brequinar treatment and found decrease of labeled intermediates from *de novo* pyrimidine synthesis pathway, including orotate or UMP by Brequinar treatment (Fig. 6D). These data suggest on-target effects of these drug treatments in our TNBC model.

Downloaded from cancerres.aacrjournals.org on December 16, 2021. © 2021 American Association for Cancer Research.

Author Manuscript Published OnlineFirst on December 15, 2021; DOI: 10.1158/0008-5472.CAN-21-2745
Author manuscripts have been peer reviewed and accepted for publication but have not yet been edited.

To examine the therapeutic efficacy of targeting pyrimidine and glutamine metabolism *in vivo*, we first separately implanted two basal-like TNBC cell lines, fast-growing HCC1806 and slower-growing MDA-MB-468, orthotopically into the mammary fat pad in NSG mice. Upon tumor growth to approximately 150 mm^3 for HCC1806 and 50 mm^3 for MDA-MB-568, mice were randomized into control, CB-839, Brequinar, and combined treatment groups. CB-839 was administered continuously in a CB-839 formulated chow (1400mg/kg diet dose) and Brequinar was given intraperitoneally (20mg/kg body weight) twice a week (Fig. 6, E and J). We monitored the tumor growth over time and recorded the survival days.

We did not observe overt toxicity reflected by relatively body weight change for these single and combination treatments (Supplementary Fig. S9A). CB-839 or Brequinar single treatment led to a decrease in HCC1806 tumor growth (Fig. 6F), and improved survival compared to the control group (Fig. 6G). The combination of both drugs further suppressed the tumor growth over time and significantly prolonged the survival compared to the control or any single treatment group (Fig. 6, F and G). In order to examine the effect of the combination drug treatment on tumor metabolism *in vivo*, we treated HCC1806 tumor bearing mice with or without the combined drugs for 10 days followed by tumor collection and targeted metabolite analysis by LC-MS. We found that metabolites related to the CB-839 or Brequinar targeted pathways were significantly altered by the combined drug treatment (Fig. 6A), e.g., glutamine was accumulated, whereas its downstream metabolites including glutamate, TCA cycle intermediates, GSH, and GSSG were decreased (Fig. 6H). On the other hand, the upstream metabolite of DHODH enzyme, dihydroorotate was dramatically accumulated

Downloaded from cancerres.aacrjournals.org on December 16, 2021. © 2021 American Association for Cancer Research.

Author Manuscript Published OnlineFirst on December 15, 2021; DOI: 10.1158/0008-5472.CAN-21-2745
Author manuscripts have been peer reviewed and accepted for publication but have not yet been edited.

concomitant with decreased downstream pyrimidine nucleotides (Fig. 6I). Therefore, not only did these analyses demonstrate a drug on-target effect, but also provide a proof-of-principle for combining the CB-839 with Brequinar *in vivo*. We repeated the same set of xenograft experiments above in another TNBC/basal-like breast cancer cell line MDA-MB-468 and found a very similar pattern (Fig.6, J-N; Supplementary Fig. S9B, S10, A-F).

To further test the efficacy of these drugs in a more physiologically relevant model, we treated WHIM2, a representative basal-like TNBC PDX model (40) (Fig. 6O). Our results showed that either treatment showed anti-tumor efficacy, and the combined treatment caused further decreased tumor growth and prolonged survival when compared to control group or single drug treatment group (Fig. 6, P and Q). To further address the metabolite change in tumors over time, metabolites in the PDX tumors with acute (24 hour) or middle-term (15 days) single drug treatment were measured, which further demonstrated the on-target efficacy of these drugs reflected by related metabolite change (Fig. 6, R and S).

Comparison of pyrimidine metabolism inhibition with standard chemotherapy

Previous studies targeted the pyrimidine synthesis in the PTEN-mutant or chemotherapy resistant tumors, which showed promising therapeutic outcomes in TNBC (10, 41). Given that Brequinar showed significant antitumor efficacy in our TNBC tumor models, we further sought to compare the therapeutic efficacy of Brequinar with standard chemotherapy in immune-competent TNBC models. The Trp53-null genetically engineered transplant mouse model, which produces phenotypically and genomically diverse tumors, can be classified into three major subtypes/classes based on gene expression profiles: p53null-Basal, Claudin-low, and p53null-Luminal (22). Here, we

Downloaded from cancerres.aacrjournals.org on December 16, 2021. © 2021 American Association for Cancer Research.

Author Manuscript Published OnlineFirst on December 15, 2021; DOI: 10.1158/0008-5472.CAN-21-2745
Author manuscripts have been peer reviewed and accepted for publication but have not yet been edited.

utilized 5 validated p53-null serial transplant TNBC models, namely 2336R, 9263-3, 2224L, 2225L, and T-11, to compare the efficacy of Brequinar with standard chemotherapy. In the chemotherapy (Carbo/Tax) treatment group, tumor bearing mice were intraperitoneally administered Paclitaxel (10mg/kg) and Carboplatin (50 mg/kg) once per week (Fig. 7A). Tumor growth was monitored and tumor volume was measured upon the control group reached tumor burden, and survival studies were conducted with continued drug treatment over time. We found that each p53-null murine tumor model showed different levels of sensitivity to Brequinar or Carbo/Tax treatment (Fig. 7, B-F). For the Brequinar treatment, all models (2336R, 9263-3R, 2224L, 2225L, and T-11) were sensitive with significantly decreased tumor volume and prolonged survival (Fig. 7, B-F). However, with the Carbo/Tax treatment, 3 models (2336R, 2225L, and T-11) were sensitive (Fig. 7, D-F) and 2 models (9263-3R, 2224L) were resistant (Fig. 7, B and C). More importantly, Brequinar treatment showed better therapeutic outcomes than Carbo/Tax in these models and less toxicity (Fig. 7, B-F). These data suggest that pyrimidine metabolism inhibition by Brequinar shows comparable, or even better, antitumor activity compared with a standard chemotherapy doublet in this array of heterogenous murine TNBC models. Further, to explore the possibility of combination of pyrimidine inhibition with immunotherapy, we treated an immunogenic 4T1 mouse model with Brequinar and/or anti-PD-1 treatment. However, our current data showed that the combination of Brequinar and anti-PD-1 antibody did not improve overall tumor inhibition (Supplementary Fig. S11A) or survival (Supplementary Fig. S11B) in this model, which is consistent with our immune-related signature lack of association with our TNBC-high metabolite-determined group (Supplementary Fig. S7).

Downloaded from cancerres.aacrjournals.org on December 16, 2021. © 2021 American Association for Cancer Research.

Author Manuscript Published OnlineFirst on December 15, 2021; DOI: 10.1158/0008-5472.CAN-21-2745
Author manuscripts have been peer reviewed and accepted for publication but have not yet been edited.

Discussion

Our study provides a comprehensive metabolic profiling and gene expression analysis of breast cancers comparing TNBC and ER^+ patient tumors, PDXs, and cell lines *in vivo*. Based on the data generated from this study, we developed a public, interactive data visualization portal (http://brcametab.org). This portal enables users to interactively explore associations between metabolite abundances and gene expression level within different clinical and PAM50 subtypes of breast cancer samples. We found two distinctive groups of patient samples stratified by unsupervised analyses of the untargeted metabolite data. One of these groups, which was comprised of normal breast tissues, ER^+ and some TNBC tumors, was denoted the "Lipid/Fatty Acid-Enriched" phenotype because of its high enrichment for lipid/fatty acid related pathways. Of note, the majority of TNBC tumors and all PDXs tested were featured in the second group, denoted "Nucleotide/Carbohydrate-Enriched" because of its high levels of nucleotide, carbohydrate, and energy metabolism pathways. Furthermore, we found very a strong gene expression signature correlated with each metabolite signature, suggesting that these metabolites may be used as a strong predictor for high cell proliferation rates in breast cancer patients. Therapeutically, we tested the efficacy in different models of TNBC xenografts by blocking the pyrimidine metabolism or glutamine/glutamate metabolism pathways that are robustly upregulated in TNBCs. We also provided the rationale for inhibiting these two pathways through combination treatments, showing improved therapeutic outcomes when compared with single drug treatment *in vivo*. Although we focused on the therapeutic opportunities in the

Downloaded from cancerres.aacrjournals.org on December 16, 2021. © 2021 American Association for Cancer Research.

Author Manuscript Published OnlineFirst on December 15, 2021; DOI: 10.1158/0008-5472.CAN-21-2745
Author manuscripts have been peer reviewed and accepted for publication but have not yet been edited.

nucleotide/carbohydrate enriched TNBC, the lipid/fatty acid enrichment in the ER^+ or part of TNBCs remains intriguing and warrants further investigation.

Previous research has attempted to identify therapeutic vulnerabilities in metabolic pathways in TNBCs. For example, by using cell line models grown *in vitro*, researchers showed that a core set of TCA cycle and fatty acid pathways could be important for TNBC cell line survival (42). The potential caveat is that this study only used the cell line grown *in vitro*, which, as we show in our current study, displayed distinctly different metabolic profiles when compared to breast tumor patient samples or even these same cell lines grown *in vivo* (Fig. 3A). Another study using mouse breast cancer models, including PyMT, Wnt1, Neu and C3-TAg, showed that C3-TAg, a mouse TNBC tumor line with gene expression similar to human basal-like subtype tumors (22), displayed decreased lipids and γ-glutamyl amino acids with increased glycogen metabolites (43). This study suggests that increased glutathione production or decreased glutathione breakdown may be important in TNBC, which is consistent with the findings in our study (Fig. 1E and Fig. S8B). Another study used 204 ER^+ and 67 ER^- breast tumors for metabolomics and revealed that 19 metabolites showed different levels between these two clinical subtypes (44). The metabolite changes included increased alanine, 2-hydroxyglutarate (2-HG), glutamate, and decreased glutamine in the ER^- breast tumors. This latter finding is consistent with our finding that glutamate metabolism is enriched in TNBC breast tumors. Another study using a limited number of TCGA breast tumor samples showed that ER^- breast tumors displayed high levels of 2-HG and tryptophan metabolite kynurenine (45). Our study also revealed significant increase in 2-HG in TNBC tumors, PDXs, as well as TNBC cells lines grown *in vivo* (Fig. 3E; and Fig. S2C).

Downloaded from cancerres.aacrjournals.org on December 16, 2021. © 2021 American Association for Cancer Research.

Author Manuscript Published OnlineFirst on December 15, 2021; DOI: 10.1158/0008-5472.CAN-21-2745
Author manuscripts have been peer reviewed and accepted for publication but have not yet been edited.

It was also reported that Warburg-like metabolism was enriched in breast tumors exemplified by the increase Glut-1 expression (28, 46). In accordance with this finding, we also found increased levels of lactate in TNBC tumors and PDXs compared to ER^+ breast tumors. Lactate is one of the most important metabolites involved in glycolysis and has been reported to drive cancer progression in different cancer settings (47-49). Its enrichment in the TNBC samples cross-validated our metabolomics results. Besides these, we also see that other metabolites involved in glutamate and pyrimidine metabolism were increased in TNBC tumors, including glutamate, succinate, fumarate, and UMP etc. Therefore, it is reasonable to speculate that these metabolites may promote cell proliferation in a similar fashion as lactate. Future investigation will need to be carried out to examine their roles in driving TNBC tumor progression.

Our study is one of the very few that have integrated metabolomics with gene expression analysis in breast cancer. It has long been debated whether metabolite dysregulation may play a role in driving breast cancer or whether metabolites may be just the product of dysregulated cell proliferation. Here, we performed integrated analysis for the metabolomics and gene expression for TNBC tumors and PDXs, which showed promising implications. First, hierarchical clustering of the patient metabolomics data divided tumor samples into two distinctive clusters. The small subset of TNBC patient tumors clustered with ER^+ or normal tissues showed a different metabolic pattern compared with the other TNBC tumors, an observation that highlights how the clinically defined TNBC group is diverse on a molecular level, and that analyses strictly using clinically defined groups can mask important heterogeneity in TNBC. Second, the cluster enriched with TNBC and PDXs showed distinctive gene expression differences

Downloaded from cancerres.aacrjournals.org on December 16, 2021. © 2021 American Association for Cancer Research.

Author Manuscript Published OnlineFirst on December 15, 2021; DOI: 10.1158/0008-5472.CAN-21-2745
Author manuscripts have been peer reviewed and accepted for publication but have not yet been edited.

compared to the other cluster enriched with ER^+ breast tumors, suggesting we can further use a gene expression profile to define these metabolically distinct patient subsets. It is important to note that in the top 200 gene signature comparison between metabolite-defined clusters, the gene signature derived from the Nucleotide/Carbohydrate-Enriched cluster correlated highly with many previously defined cell proliferation signatures that contain many of the enzymes for nucleotide synthesis, thus showing very different and objective 'omics' methods each landing on a common and strong biological phenotype. One limitation of our study is that, with current technique, we could not dissect whether the metabolite signature was derived from tumor cells or stromal cells.

Chemotherapy still remains the standard of care for TNBC patients, although new immunotherapy are beginning to have a role in the metastatic setting. Chemotherapy is effective in early stage TNBC, whereas late stage patients and/or patients that develop metastases are more resistant to chemotherapy, leading to a poor survival (50). It is imperative to identify new therapeutic vulnerabilities in TNBC that may be able to, either alone or in combination, improve the survival rate for these patients. Although dysregulated metabolism is considered to be important for cancer progression, including in TNBCs, it lacks systemic characterization. In our study, we performed systemic profiling of metabolomics and gene expression for relevant TNBC tumor samples as well as PDXs. In conclusion, we identify two therapeutic vulnerabilities present within the often-deadly TNBC cells, and a biomarker in the form of both metabolic and genetic signatures, to identify these patients. Future studies will explore the possibilities of using these inhibitors, alone, together, and/or in combination with chemotherapy, to examine

Downloaded from cancerres.aacrjournals.org on December 16, 2021. © 2021 American Association for Cancer Research.

Author Manuscript Published OnlineFirst on December 15, 2021; DOI: 10.1158/0008-5472.CAN-21-2745
Author manuscripts have been peer reviewed and accepted for publication but have not yet been edited.

whether specifically targeting pyrimidine and/or glutamate metabolism can be used as a true biologically targeted therapeutic approach for patients with TNBC.

Acknowledgments

We thank all members of the Zhang and Perou laboratories for helpful discussions and suggestions. We thank Drs. Srinivas Malladi, Kangsan Kim and Pravat Parida from UT Southwestern for their kind helps and suggestions during revision. This work was supported by Cancer Prevention and Research Institute of Texas (Q. Zhang, CPRIT, RR190058) and ACS Research Scholar Award (Q. Zhang, RSG-18-059-01-TBE), NCI Breast SPORE program (C.M. Perou, P50-CA58223), National Cancer Institute (C.M. Perou, R01-CA148761) and BCRF (C.M. Perou).

Author contributions

C.M.P., Q.Z., and C.L. participated in the conception and design of the experiments. C.L. performed the metabolite extraction and data interpretation. J.L. and H. V. performed the metabolite LC/MS measurement and annotation. C.R.G. and C.L. performed the RNA-sequencing and analysis. C.L. and K.R.M. performed the animal study. C.L. and A.K. performed the isotope tracing experiments. C.F. performed the data processing, bioinformatic and statistical analysis. R.J.D., J.W.L. and S.K.M. provided critical advice and comments. C.L., Q.Z., C.R.G., and C.M.P. wrote and revised the paper with comments from all authors.

Downloaded from cancerres.aacrjournals.org on December 16, 2021. © 2021 American Association for Cancer Research.

Author Manuscript Published OnlineFirst on December 15, 2021; DOI: 10.1158/0008-5472.CAN-21-2745
Author manuscripts have been peer reviewed and accepted for publication but have not yet been edited.

Downloaded from cancerres.aacrjournals.org on December 16, 2021. © 2021 American Association for Cancer Research.

Author Manuscript Published OnlineFirst on December 15, 2021; DOI: 10.1158/0008-5472.CAN-21-2745
Author manuscripts have been peer reviewed and accepted for publication but have not yet been edited.

References

1. Sung H, Ferlay J, Siegel RL, Laversanne M, Soerjomataram I, Jemal A, et al. Global Cancer Statistics 2020: GLOBOCAN Estimates of Incidence and Mortality Worldwide for 36 Cancers in 185 Countries. CA Cancer J Clin. 2021;71:209-49.

2. Anders CK, Carey LA. Biology, metastatic patterns, and treatment of patients with triple-negative breast cancer. Clin Breast Cancer. 2009;9 Suppl 2:S73-81.

3. Hanahan D, Weinberg RA. Hallmarks of cancer: the next generation. Cell. 2011;144:646-74.

4. Ward PS, Thompson CB. Metabolic reprogramming: a cancer hallmark even warburg did not anticipate. Cancer cell. 2012;21:297-308.

5. Kroemer G, Pouyssegur J. Tumor cell metabolism: cancer's Achilles' heel. Cancer cell. 2008;13:472-82.

6. Vander Heiden MG. Targeting cancer metabolism: a therapeutic window opens. Nature reviews Drug discovery. 2011;10:671-84.

7. Pavlova NN, Thompson CB. The Emerging Hallmarks of Cancer Metabolism. Cell metabolism. 2016;23:27-47.

8. Lien EC, Lyssiotis CA, Juvekar A, Hu H, Asara JM, Cantley LC, et al. Glutathione biosynthesis is a metabolic vulnerability in PI(3)K/Akt-driven breast cancer. Nature cell biology. 2016;18:572-8.

9. Brown KK, Spinelli JB, Asara JM, Toker A. Adaptive Reprogramming of De Novo Pyrimidine Synthesis Is a Metabolic Vulnerability in Triple-Negative Breast Cancer. Cancer discovery. 2017;7:391-9.

10. Mathur D, Stratikopoulos E, Ozturk S, Steinbach N, Pegno S, Schoenfeld S, et al. PTEN Regulates Glutamine Flux to Pyrimidine Synthesis and Sensitivity to Dihydroorotate Dehydrogenase Inhibition. Cancer Discov. 2017;7:380-90.

11. Liao C, Zhang Y, Fan C, Herring LE, Liu J, Locasale JW, et al. Identification of BBOX1 as a Therapeutic Target in Triple-Negative Breast Cancer. Cancer discovery. 2020;10:1706-21.

12. Liu X, Ser Z, Locasale JW. Development and quantitative evaluation of a high-resolution metabolomics technology. Anal Chem. 2014;86:2175-84.

Downloaded from cancerres.aacrjournals.org on December 16, 2021. © 2021 American Association for Cancer Research.

Author Manuscript Published OnlineFirst on December 15, 2021; DOI: 10.1158/0008-5472.CAN-21-2745
Author manuscripts have been peer reviewed and accepted for publication but have not yet been edited.

13. Kanehisa M, Goto S. KEGG: kyoto encyclopedia of genes and genomes. Nucleic Acids Res. 2000;28:27-30.

14. Wishart DS, Feunang YD, Marcu A, Guo AC, Liang K, Vazquez-Fresno R, et al. HMDB 4.0: the human metabolome database for 2018. Nucleic Acids Res. 2018;46:D608-D17.

15. Chong J, Wishart DS, Xia J. Using MetaboAnalyst 4.0 for Comprehensive and Integrative Metabolomics Data Analysis. Curr Protoc Bioinformatics. 2019;68:e86.

16. Hakimi AA, Reznik E, Lee CH, Creighton CJ, Brannon AR, Luna A, et al. An Integrated Metabolic Atlas of Clear Cell Renal Cell Carcinoma. Cancer Cell. 2016;29:104-16.

17. Parker JS, Mullins M, Cheang MC, Leung S, Voduc D, Vickery T, et al. Supervised risk predictor of breast cancer based on intrinsic subtypes. Journal of clinical oncology : official journal of the American Society of Clinical Oncology. 2009;27:1160-7.

18. Zhao X, Rodland EA, Tibshirani R, Plevritis S. Molecular subtyping for clinically defined breast cancer subgroups. Breast Cancer Res. 2015;17:29.

19. Nielsen TO, Parker JS, Leung S, Voduc D, Ebbert M, Vickery T, et al. A comparison of PAM50 intrinsic subtyping with immunohistochemistry and clinical prognostic factors in tamoxifen-treated estrogen receptor-positive breast cancer. Clin Cancer Res. 2010;16:5222-32.

20. Leone RD, Zhao L, Englert JM, Sun IM, Oh MH, Sun IH, et al. Glutamine blockade induces divergent metabolic programs to overcome tumor immune evasion. Science. 2019;366:1013-21.

21. Biancur DE, Paulo JA, Malachowska B, Del Rey MQ, Sousa CM, Wang XX, et al. Compensatory metabolic networks in pancreatic cancers upon perturbation of glutamine metabolism. Nature Communications. 2017;8.

22. Pfefferle AD, Herschkowitz JI, Usary J, Harrell JC, Spike BT, Adams JR, et al. Transcriptomic classification of genetically engineered mouse models of breast cancer identifies human subtype counterparts. Genome Biol. 2013;14:R125.

Downloaded from cancerres.aacrjournals.org on December 16, 2021. © 2021 American Association for Cancer Research.

23. Tusher VG, Tibshirani R, Chu G. Significance analysis of microarrays applied to the ionizing radiation response. Proceedings of the National Academy of Sciences of the United States of America. 2001;98:5116-21.

24. Li S, Shen D, Shao J, Crowder R, Liu W, Prat A, et al. Endocrine-therapy-resistant ESR1 variants revealed by genomic characterization of breast-cancer-derived xenografts. Cell Rep. 2013;4:1116-30.

25. Zhang Q, Gu J, Li L, Liu J, Luo B, Cheung HW, et al. Control of cyclin D1 and breast tumorigenesis by the EglN2 prolyl hydroxylase. Cancer Cell. 2009;16:413-24.

26. Zhang J, Wang C, Chen X, Takada M, Fan C, Zheng X, et al. EglN2 associates with the NRF1-PGC1alpha complex and controls mitochondrial function in breast cancer. The EMBO journal. 2015;34:2953-70.

27. Schimke RT. Enzymes of Arginine Metabolism in Mammalian Cell Culture. I. Repression of Argininosuccinate Synthetase and Argininosuccinase. The Journal of biological chemistry. 1964;239:136-45.

28. Brauer HA, Makowski L, Hoadley KA, Casbas-Hernandez P, Lang LJ, Roman-Perez E, et al. Impact of tumor microenvironment and epithelial phenotypes on metabolism in breast cancer. Clin Cancer Res. 2013;19:571-85.

29. Cancer Genome Atlas N. Comprehensive molecular portraits of human breast tumours. Nature. 2012;490:61-70.

30. Osborne CK, Schiff R. Mechanisms of endocrine resistance in breast cancer. Annu Rev Med. 2011;62:233-47.

31. Newman AM, Liu CL, Green MR, Gentles AJ, Feng W, Xu Y, et al. Robust enumeration of cell subsets from tissue expression profiles. Nature methods. 2015;12:453-7.

32. Hollern DP, Xu N, Thennavan A, Glodowski C, Garcia-Recio S, Mott KR, et al. B Cells and T Follicular Helper Cells Mediate Response to Checkpoint Inhibitors in High Mutation Burden Mouse Models of Breast Cancer. Cell. 2019;179:1191-206 e21.

33. Curtis C, Shah SP, Chin SF, Turashvili G, Rueda OM, Dunning MJ, et al. The genomic and transcriptomic architecture of 2,000 breast tumours reveals novel subgroups. Nature. 2012;486:346-52.

Downloaded from cancerres.aacrjournals.org on December 16, 2021. © 2021 American Association for Cancer Research.

34. Harrell JC, Prat A, Parker JS, Fan C, He X, Carey L, et al. Genomic analysis identifies unique signatures predictive of brain, lung, and liver relapse. Breast Cancer Res Treat. 2012;132:523-35.

35. Brueffer C, Vallon-Christersson J, Grabau D, Ehinger A, Hakkinen J, Hegardt C, et al. Clinical Value of RNA Sequencing-Based Classifiers for Prediction of the Five Conventional Breast Cancer Biomarkers: A Report From the Population-Based Multicenter Sweden Cancerome Analysis Network-Breast Initiative. JCO Precis Oncol. 2018;2.

36. Gatza ML, Silva GO, Parker JS, Fan C, Perou CM. An integrated genomics approach identifies drivers of proliferation in luminal-subtype human breast cancer. Nat Genet. 2014;46:1051-9.

37. Huang DW, Sherman BT, Lempicki RA. Systematic and integrative analysis of large gene lists using DAVID bioinformatics resources. Nat Protoc. 2009;4:44-57.

38. Altman BJ, Stine ZE, Dang CV. From Krebs to clinic: glutamine metabolism to cancer therapy. Nat Rev Cancer. 2016;16:749.

39. Reinfeld BI, Madden MZ, Wolf MM, Chytil A, Bader JE, Patterson AR, et al. Cell-programmed nutrient partitioning in the tumour microenvironment. Nature. 2021;593:282-8.

40. Ding L, Ellis MJ, Li S, Larson DE, Chen K, Wallis JW, et al. Genome remodelling in a basal-like breast cancer metastasis and xenograft. Nature. 2010;464:999-1005.

41. Brown KK, Spinelli JB, Asara JM, Toker A. Adaptive Reprogramming of De Novo Pyrimidine Synthesis Is a Metabolic Vulnerability in Triple-Negative Breast Cancer (vol 7, pg 391, 2017). Cancer Discov. 2017;7:782-.

42. Lanning NJ, Castle JP, Singh SJ, Leon AN, Tovar EA, Sanghera A, et al. Metabolic profiling of triple-negative breast cancer cells reveals metabolic vulnerabilities. Cancer Metab. 2017;5:6.

43. Dai C, Arceo J, Arnold J, Sreekumar A, Dovichi NJ, Li J, et al. Metabolomics of oncogene-specific metabolic reprogramming during breast cancer. Cancer Metab. 2018;6:5.

44. Budczies J, Brockmoller SF, Muller BM, Barupal DK, Richter-Ehrenstein C, Kleine-Tebbe A, et al. Comparative metabolomics of estrogen receptor positive and

Downloaded from cancerres.aacrjournals.org on December 16, 2021. © 2021 American Association for Cancer Research.

Author Manuscript Published OnlineFirst on December 15, 2021; DOI: 10.1158/0008-5472.CAN-21-2745
Author manuscripts have been peer reviewed and accepted for publication but have not yet been edited.

estrogen receptor negative breast cancer: alterations in glutamine and beta-alanine metabolism. J Proteomics. 2013;94:279-88.

45. Tang X, Lin CC, Spasojevic I, Iversen ES, Chi JT, Marks JR. A joint analysis of metabolomics and genetics of breast cancer. Breast cancer research : BCR. 2014;16:415.

46. Sun X, Wang M, Wang M, Yu X, Guo J, Sun T, et al. Metabolic Reprogramming in Triple-Negative Breast Cancer. Frontiers in oncology. 2020;10:428.

47. Hirschhaeuser F, Sattler UG, Mueller-Klieser W. Lactate: a metabolic key player in cancer. Cancer research. 2011;71:6921-5.

48. Faubert B, Li KY, Cai L, Hensley CT, Kim J, Zacharias LG, et al. Lactate Metabolism in Human Lung Tumors. Cell. 2017;171:358-71 e9.

49. Tasdogan A, Faubert B, Ramesh V, Ubellacker JM, Shen B, Solmonson A, et al. Metabolic heterogeneity confers differences in melanoma metastatic potential. Nature. 2020;577:115-20.

50. Garrido-Castro AC, Lin NU, Polyak K. Insights into Molecular Classifications of Triple-Negative Breast Cancer: Improving Patient Selection for Treatment. Cancer discovery. 2019;9:176-98.

Downloaded from cancerres.aacrjournals.org on December 16, 2021. © 2021 American Association for Cancer Research.

Author Manuscript Published OnlineFirst on December 15, 2021; DOI: 10.1158/0008-5472.CAN-21-2745
Author manuscripts have been peer reviewed and accepted for publication but have not yet been edited.

Figure legends

Figure 1. Metabolic profiling in tumors from breast cancer patient and PDXs.

A, Schematic of the experimental design for untargeted global metabolomics analysis in ER^+, TNBC breast cancer patient tumors and two TNBC patient-derived xenografts (PDXs) tumors. **B,** Pie chart shows the number of metabolites identified and annotated in all samples. The annotated metabolites all with a registered ID either from the Kyoto Encyclopedia of Genes and Genomes (KEGG) database or the Human Metabolome Database (HMDB) which can be further used for pathway analysis. **C,** Unsupervised hierarchical clustering heatmap examines global metabolic profiles in 31 ER^+/TNBC patient tumor samples and PDX tumors by using the normalized metabolite intensity. Note the cluster divides the samples in two major metabolic clusters (Cluster 1 and Cluster 2). Clinical subtype and PAM50 subtype for each sample are showed. Selected classes of metabolites are highlighted. **D,** Pie chart shows the metabolites that are significant increase in the Cluster 1 or Cluster 2 samples based on the SAM analysis (q-value<0.05). **E,** KEGG pathway-based differential abundance (DA) analysis using the significant changed metabolites between Cluster 1 and 2. The DA score reflects the average, gross changes for all detected metabolites in a pathway. A score of 1 indicates all measured metabolites in the pathway increase in the Cluster 2 versus Cluster 1, and score of -1 indicates all measured metabolites in a pathway decrease. Pathways with no less than two measured metabolites were used for DA score calculation based on the detection capability for some important pathways. **F-I,** Relative normalized intensity levels of representative metabolites, involved in energy production (**F**), nucleotides (**G**), lipids/fatty acids (**H**), and amino acids (**I**), that were differentially abundant between

Downloaded from cancerres.aacrjournals.org on December 16, 2021. © 2021 American Association for Cancer Research.

Author Manuscript Published OnlineFirst on December 15, 2021; DOI: 10.1158/0008-5472.CAN-21-2745
Author manuscripts have been peer reviewed and accepted for publication but have not yet been edited.

metabolic clusters from panel **(C)**. Data are represented as mean ± standard error of the mean (SEM), two-tailed Student's t-test; *p<0.05, **p <0.01, ***p<0.001, ****p<0.0001.

Figure 2. Distinctive metabolism of cell lines grown *in vivo* versus *in vitro.*

A, Schematic of the experimental design for metabolic profiling of breast cancer cell lines grown *in vitro* and *in vivo* condition. Cell lines grown *in vivo* were conducted by growing and collecting tumors from three individual mice, cell line grown *in vitro* were performed in parallel in biological duplicates. **B,** Principal component analysis (PCA) of individual samples for the normalized metabolomics data in cell line grown *in vivo* and *in vitro*. **(C)** Unsupervised hierarchical clustering heatmap of normalized metabolomics data in cell line grown *in vivo* and *in vitro*. **D** and **E,** Histograms of metabolic pathway enrichment using statistical differed metabolites (SAM, q-value <0.05) that high in cells grown *in vitro* (**D**) or high in cells grown *in vitro* (**E**). All statistically significant (p<0.05) pathways were showed. **F** and **G,** Relative normalized intensity levels of representative metabolites that are significantly increased in cell line grown *in vitro* (**F**) or *in vivo* (**G**). Data are represented as mean ± standard error of the mean (SEM), two-tailed Student's t-test; *p<0.05, **p<0.01, ***p<0.001, ****p<0.0001.

Figure 3. Cell line grown *in vivo* reveals similar metabolites enrichment as in patients.

A, Unsupervised hierarchical clustering heatmap of the normalized metabolomics data by combining all cell line *in vitro* and *in vivo*, patient, PDXs samples. **B,** Pie chart shows the metabolites that are significant increase in the ER^+ or TNBC cell derived xenograft

Downloaded from cancerres.aacrjournals.org on December 16, 2021. © 2021 American Association for Cancer Research.

Author Manuscript Published OnlineFirst on December 15, 2021; DOI: 10.1158/0008-5472.CAN-21-2745
Author manuscripts have been peer reviewed and accepted for publication but have not yet been edited.

tumors based on the SAM analysis (q-value<0.05). **C** and **D,** PCA analysis (**C**) and unsupervised hierarchical clustering heatmap (**D**) of the ER^+ and TNBC cell line derived xenograft tumors using the significant changed metabolites. **E** and **F,** Relative normalized intensity levels of representative metabolites that are significantly changed in cell line grown *in vitro* versus *in vivo*. Data are represented as mean ± standard error of the mean (SEM), two-tailed Student's t-test; *p<0.05, **p<0.01, ***p<0.001, ****p<0.0001, ns, not significant .

Figure 4. Integrated analysis of transcriptional and metabolic signatures in patient tumors.

A, Schematic of the correlation analysis between metabolomics and gene expression data. **B,** The PAM50 subtype correlation with the metabolite signatures from Cluster 1 and Cluster 2 patient samples from this study. **C,** Correlation of proliferation score with the tertile median level of the two metabolite signatures from Cluster 1 and Cluster 2 patient samples. **D,** A supervised clustering heatmap of the differentially expressed (DE) genes that were highly expressed in the Cluster 1 and Cluster 2 samples. DE genes were identified by SAM analysis between the Cluster 1 and Cluster 2 samples with q-value<0.05. **E** and **F,** Histogram of gene ontology (GO) analysis showing the top 200 genes that are upregulated in Cluster 2 (**E**) or Cluster 1 (**F**). Top 15 pathways with statistical significance (p<0.05) were showed. **G** and **H,** Kaplan-Meier plotters generated by the median expression of the top 200 genes from Cluster 2 (**G**) or Cluster 1 (**H**) in three different databases.

Downloaded from cancerres.aacrjournals.org on December 16, 2021. © 2021 American Association for Cancer Research.

Author Manuscript Published OnlineFirst on December 15, 2021; DOI: 10.1158/0008-5472.CAN-21-2745
Author manuscripts have been peer reviewed and accepted for publication but have not yet been edited.

Figure 5. Pyrimidine metabolism and glutaminolysis are elevated in TNBC.

A, Metabolic pathway-based gene set enrichment analysis using the DE genes (q-value<0.05, SAM) within each metabolic cluster. All statistically significant (p<0.05) pathways were showed. **B,** Heatmap showed relative expression of genes related to pyrimidine metabolism in the patient tumors and PDXs stratified by the metabolic clusters. Genes upregulated in Cluster 2 samples are shown with statistic markers. **C,** A schematic shows the key genes for the initial steps of glutaminolysis and *de novo* pyrimidine biosynthesis. **D,** Relative gene expression of the key genes between Cluster 1 and 2 samples. **E,** Heatmap shows relative expression of genes related to glutamine metabolism and transport in the patient tumors and PDXs stratified by the metabolic clusters. Genes upregulated in Cluster 2 samples are shown with statistic markers. **F,** Schematic of key metabolites denotes metabolite abundance in tumors in Cluster 1 or Cluster 2. Significant abundant metabolites from SAM analysis (q-value <0.05) were highlighted, with metabolite in red accumulated in Cluster 2 or in blue accumulated in Cluster 1. The expected major labeling patterns of some metabolites from $^{13}C_5$- or $^{15}N_2$-glutamine isotope tracing are also showed. **G-I,** Relative abundance ratio of the downstream and upstream metabolites from glutamate to glutamine (**G**), carbamoyl-aspartate to glutamine (**H**), and carbamoyl-aspartate to aspartate (**I**), indicating the metabolic flow at the initial steps in the glutaminolysis and pyrimidine metabolism pathways in patient (left) or cell line *in vivo* (right) samples. **J-L,** Contribution of glutamine carbon to amino acids (**J**), TCA cycle and glutathione (**K**), and nucleotides (**L**) in HCC1806 TNBC xenograft tumors (n=4) infused with $^{13}C_5$-glutamine in 45 mins. **M,** Contribution of glutamine nitrogen to nucleotides in HCC1806 TNBC xenograft tumors

Downloaded from cancerres.aacrjournals.org on December 16, 2021. © 2021 American Association for Cancer Research.

Author Manuscript Published OnlineFirst on December 15, 2021; DOI: 10.1158/0008-5472.CAN-21-2745
Author manuscripts have been peer reviewed and accepted for publication but have not yet been edited.

(n=6) infused with $^{15}N_2$-glutamine in 45 mins. Data are represented as mean ± standard error of the mean (SEM), two-tailed Student's t-test; *p<0.05, **p<0.01, ***p<0.001, ****p<0.0001, ns, not significant.

Figure 6. Combination targeting the pyrimidine and glutamate metabolism in TNBC cell line xenograft and PDX model.

A, A schematic shows the key enzymes targeted by CB-839 and Brequinar in the glutamine and pyrimidine metabolism pathway and related key metabolites. **B-C,** Contribution of glutamine carbon to amino acids (**B**), the TCA cycle and glutathione (**C**) in HCC1806 tumors obtained from vehicle- and CB839-treated mice (n=4/group) at 45 min of $^{13}C_5$-glutamine bolus infusion. **D,** Contribution of glutamine nitrogen to pyrimidine nucleotides in HCC1806 tumors obtained from 3 doses of vehicle- and Brequinar-treated mice (n=5/group) at 45 min of $^{15}N_2$-glutamine bolus infusion. The expected major labeling patterns of some metabolites from $^{13}C_5$- or $^{15}N_2$-glutamine isotope tracing are showed in Figure 5F. **E-G,** Treatment strategy (**E**), tumor growth measured by volume (**F**) and survival (**G**) of the HCC1806 xenograft cohort (n=10/group). **H** and **I,** Related abundance of metabolites related to the glutamine metabolism (**H**) or pyrimidine metabolism (**I**) between the control and combination treatment group in HCC1806 xenograft tumors. Mice treated with the drugs for 10 days, then the tumors harvested for metabolite analysis. **J-L,** Treatment strategy (**J**), tumor growth measured by volume (**K**) and harvest tumor weight at 28 day (**L**) of the MDA-MB-468 xenograft cohort (Control, n=10; CB-839, n=10; Brequinar, n=9; Combined, n=8). **M** and **N,** Related abundance of key metabolites in the glutamine metabolism (**M**) or pyrimidine metabolism (**N**)

Downloaded from cancerres.aacrjournals.org on December 16, 2021. © 2021 American Association for Cancer Research.

Author Manuscript Published OnlineFirst on December 15, 2021; DOI: 10.1158/0008-5472.CAN-21-2745
Author manuscripts have been peer reviewed and accepted for publication but have not yet been edited.

pathways in MDA-MB-468 xenograft tumors in different treatment for 28 days. **O-Q,** Treatment strategy (**O**), survival (**P**) tumor growth measured by volume (**Q**) of the WHIM2 PDX xenograft cohort (Control, n=10; CB-839, n=10; Brequinar, n=10; Combined, n=7). **R** and **S,** Related abundance of key metabolites in the glutamine metabolism (**R**) or pyrimidine metabolism (**S**) pathways in the WHIM2 PDX xenograft tumors in different treatment group. Tumors harvested for metabolite analysis at 24 hours and 15 days after the treatment. Data are represented as mean ± standard error of the mean (SEM), two-tailed Student's t-test; *p<0.05, **p<0.01, ***p<0.001, ****p<0.0001, ns, not significant .

Figure 7. Comparison of pyrimidine metabolism inhibition with standard chemotherapy.

A, Treatment strategy in five p53null TNBC murine tumor line xenografts, Balb/C mice were treated with standard-of-care chemotherapy (Carboplatin+Paclitaxel) or Brequinar at indicated dose and time. **B-F,** Therapeutic outcome in terms of tumor volume change (left) or survival (right) in the 2224L (**B**), 9263-3R (**C**), 2225L (**D**), T11 (**E**), and 2336R (**F**) tumor model. Number of mice were indicated in each cohort. Data are represented as mean ± standard error of the mean (SEM), two-tailed Student's t-test.

Downloaded from cancerres.aacrjournals.org on December 16, 2021. © 2021 American Association for Cancer Research.

Author Manuscript Published OnlineFirst on December 15, 2021; DOI: 10.1158/0008-5472.CAN-21-2745
Author manuscripts have been peer reviewed and accepted for publication but have not yet been edited.

Figure 1

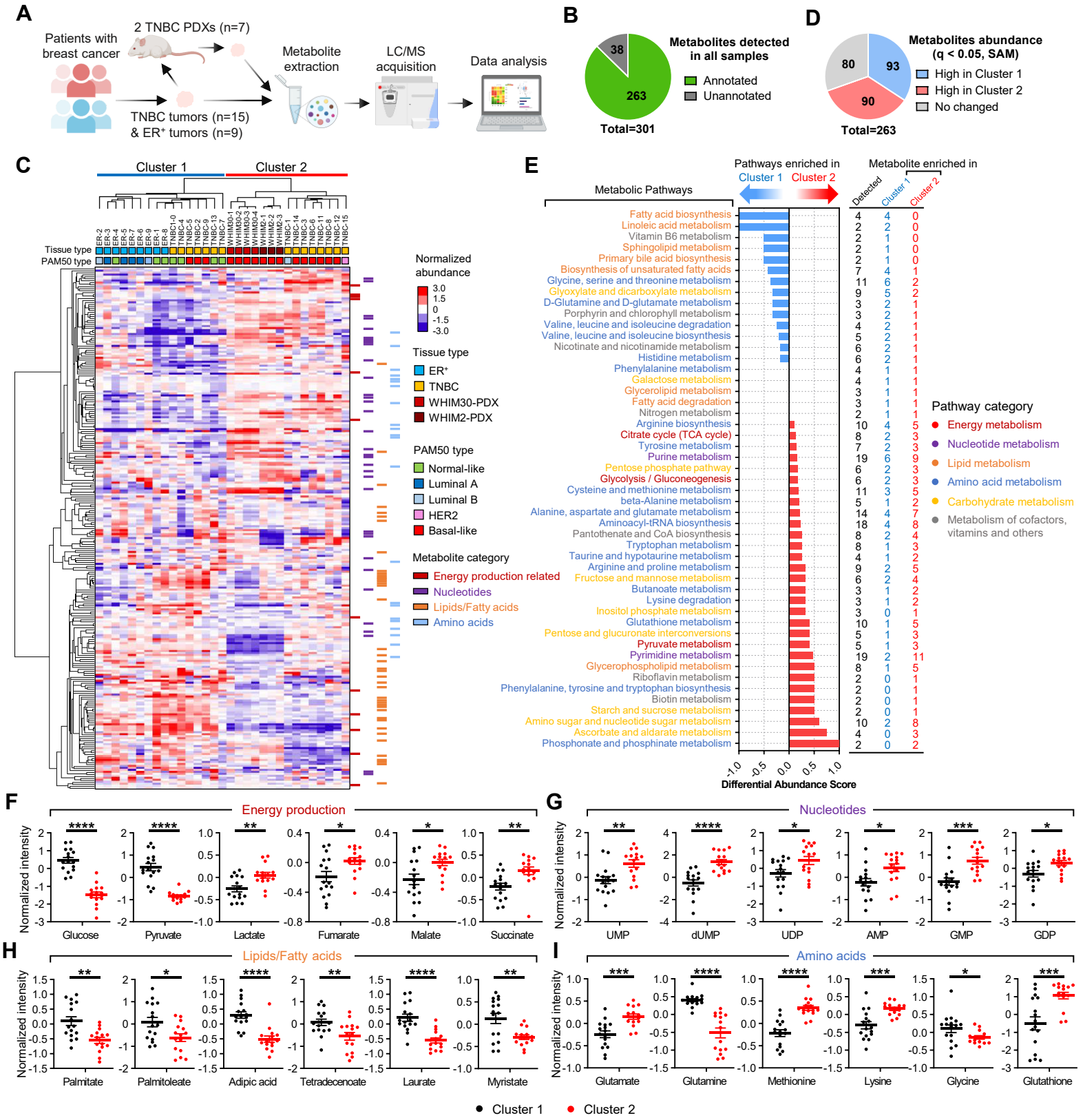

Downloaded from cancerres.aacrjournals.org on December 16, 2021. © 2021 American Association for Cancer Research.

Author Manuscript Published OnlineFirst on December 15, 2021; DOI: 10.1158/0008-5472.CAN-21-2745
Author manuscripts have been peer reviewed and accepted for publication but have not yet been edited.

Figure 2

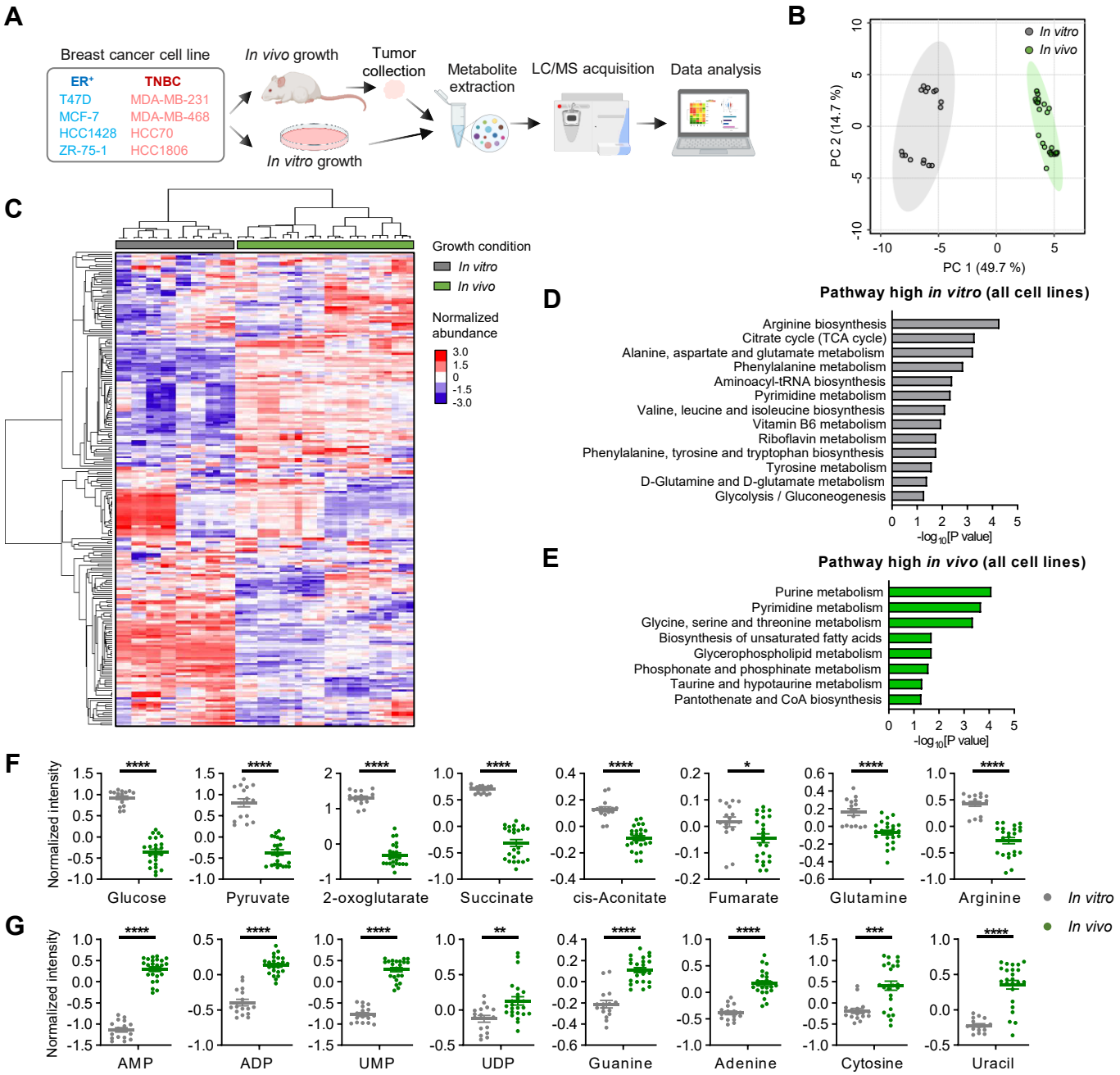

Downloaded from cancerres.aacrjournals.org on December 16, 2021. © 2021 American Association for Cancer Research.

Author Manuscript Published OnlineFirst on December 15, 2021; DOI: 10.1158/0008-5472.CAN-21-2745
Author manuscripts have been peer reviewed and accepted for publication but have not yet been edited.

Figure 3

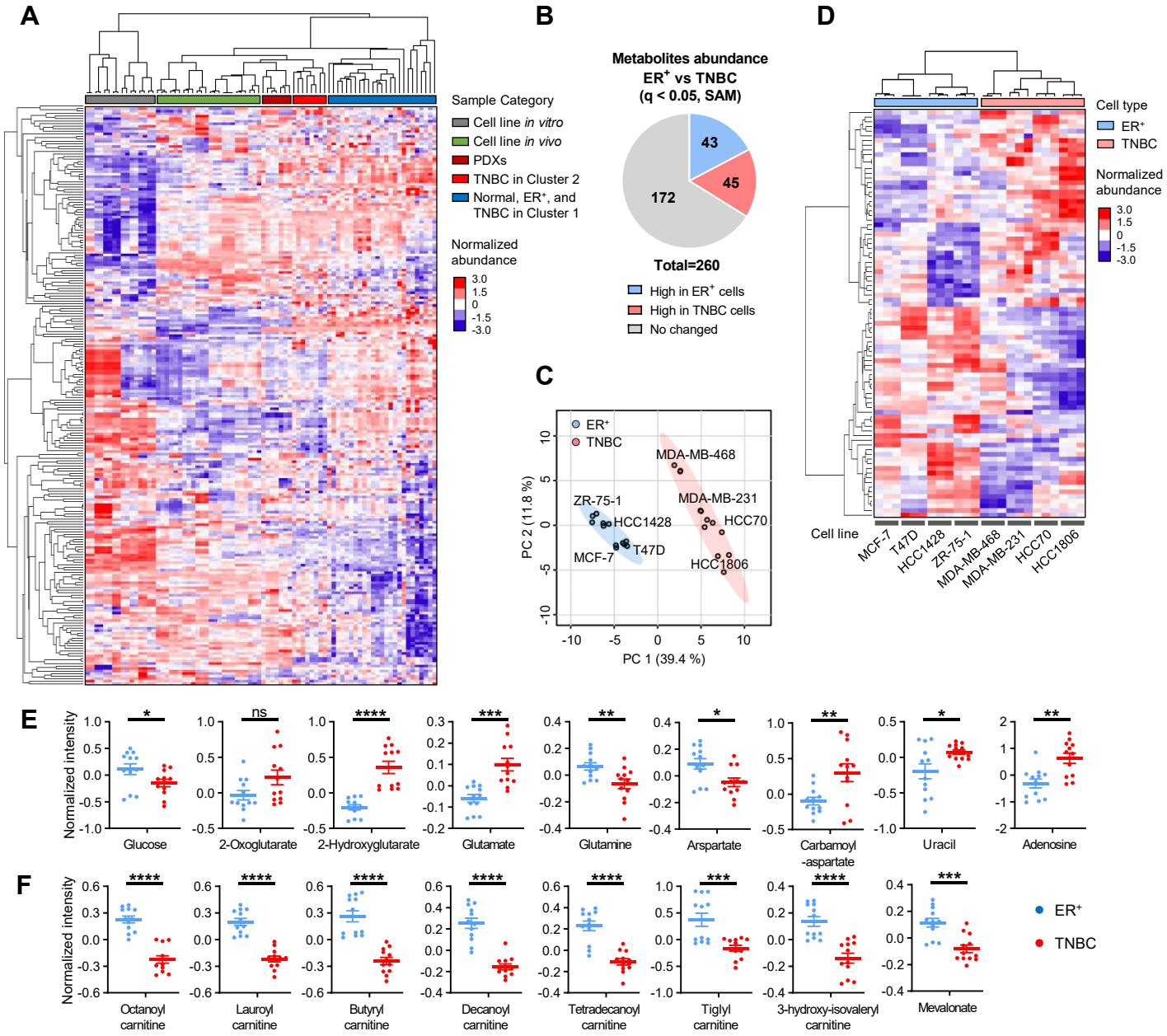

Downloaded from cancerres.aacrjournals.org on December 16, 2021. © 2021 American Association for Cancer Research.

Author Manuscript Published OnlineFirst on December 15, 2021; DOI: 10.1158/0008-5472.CAN-21-2745
Author manuscripts have been peer reviewed and accepted for publication but have not yet been edited.

Figure 4

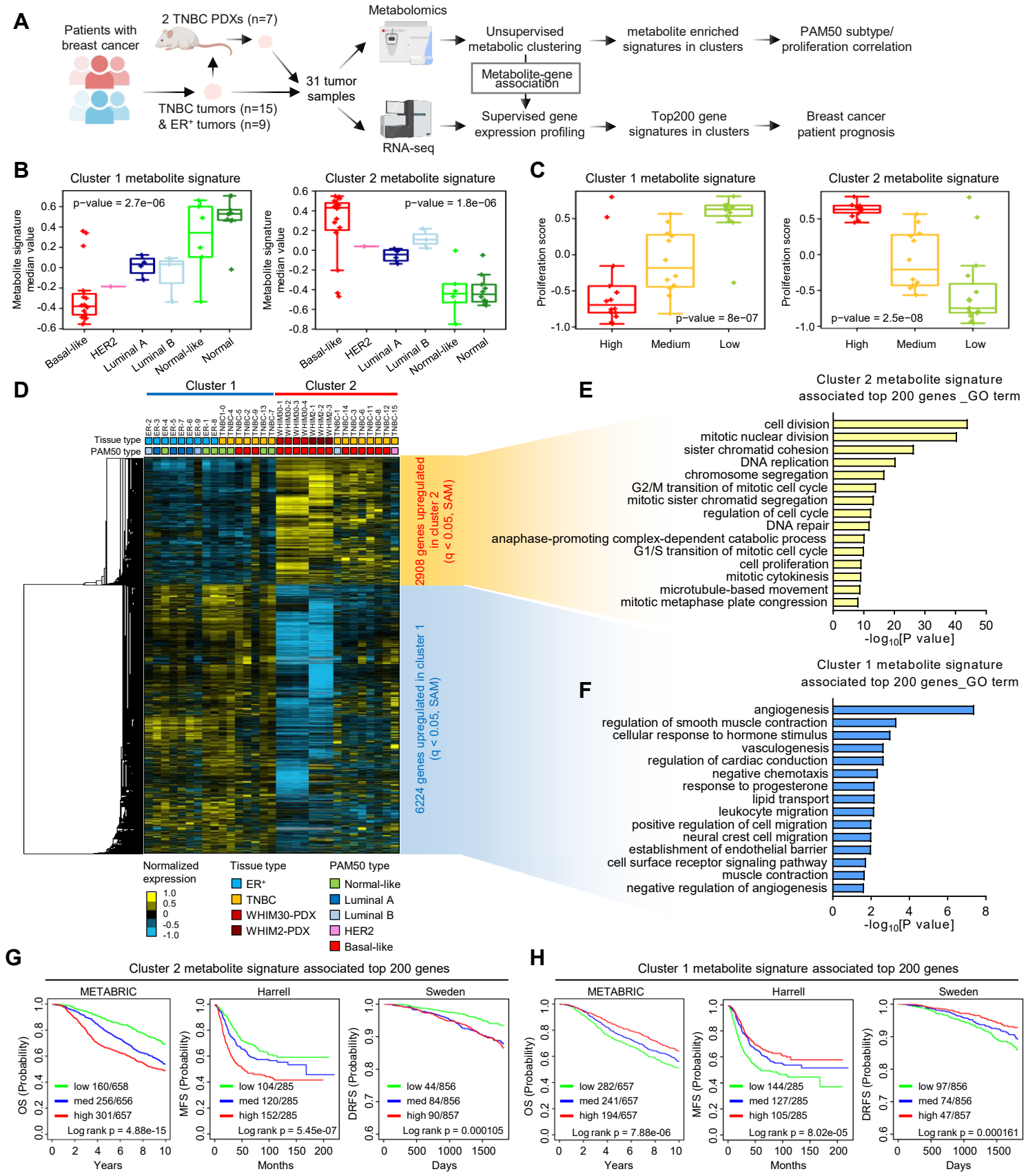

Downloaded from cancerres.aacrjournals.org on December 16, 2021. © 2021 American Association for Cancer Research.

Author Manuscript Published OnlineFirst on December 15, 2021; DOI: 10.1158/0008-5472.CAN-21-2745
Author manuscripts have been peer reviewed and accepted for publication but have not yet been edited.

Figure 5

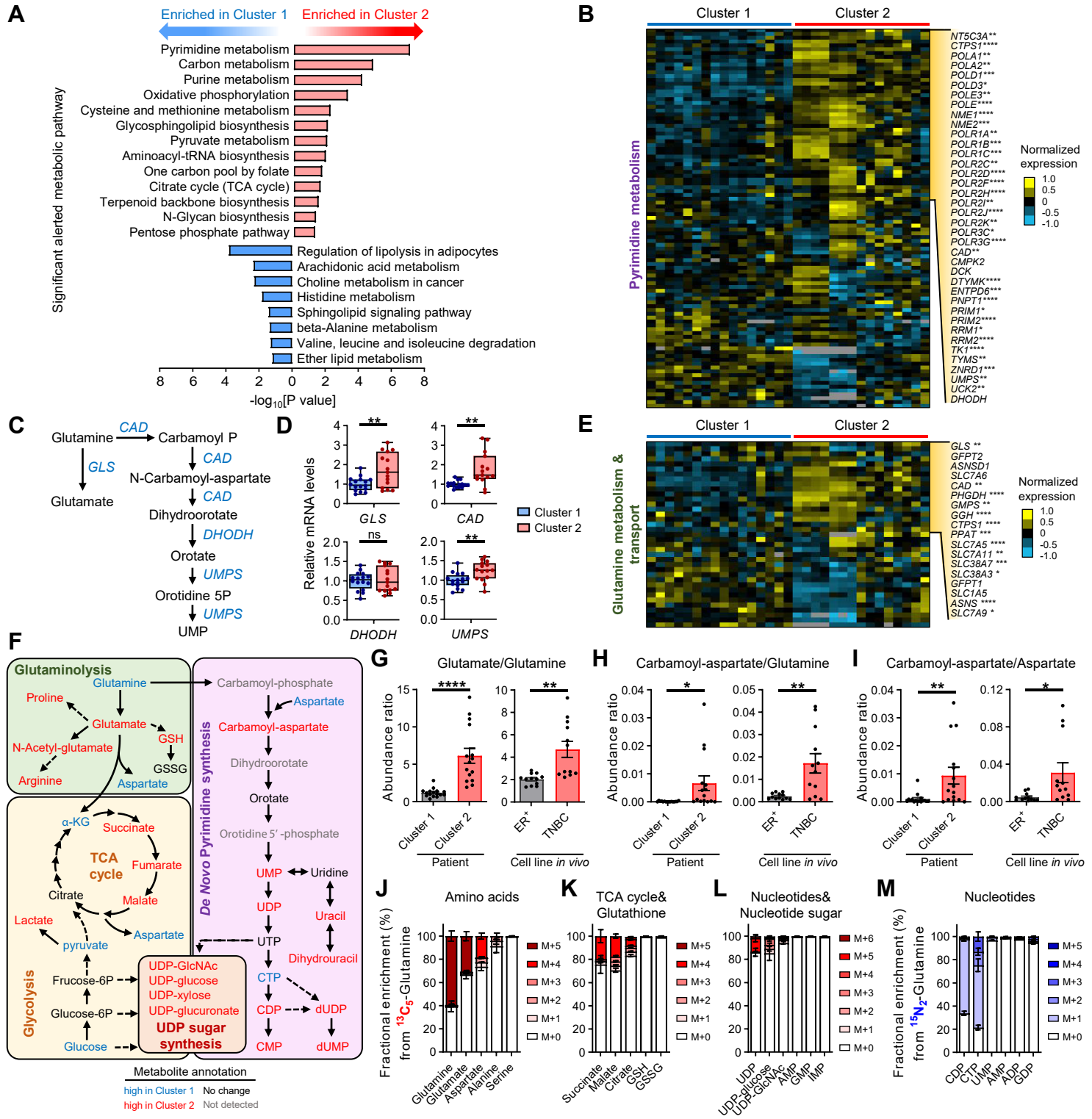

Downloaded from cancerres.aacrjournals.org on December 16, 2021. © 2021 American Association for Cancer Research.

Author Manuscript Published OnlineFirst on December 15, 2021; DOI: 10.1158/0008-5472.CAN-21-2745
Author manuscripts have been peer reviewed and accepted for publication but have not yet been edited.

Figure 6

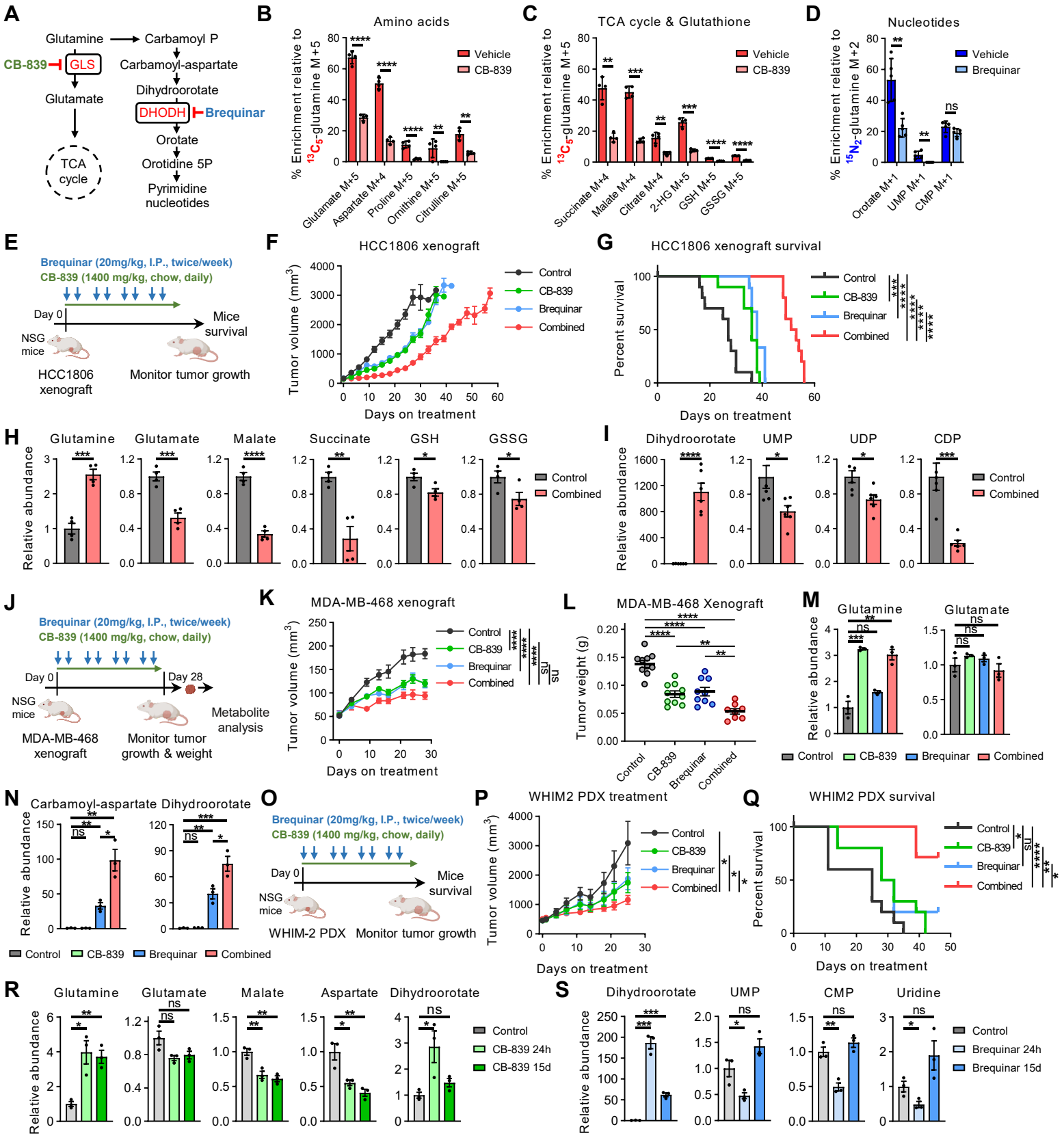

Downloaded from cancerres.aacrjournals.org on December 16, 2021. © 2021 American Association for Cancer Research.

Author Manuscript Published OnlineFirst on December 15, 2021; DOI: 10.1158/0008-5472.CAN-21-2745
Author manuscripts have been peer reviewed and accepted for publication but have not yet been edited.

Figure 7

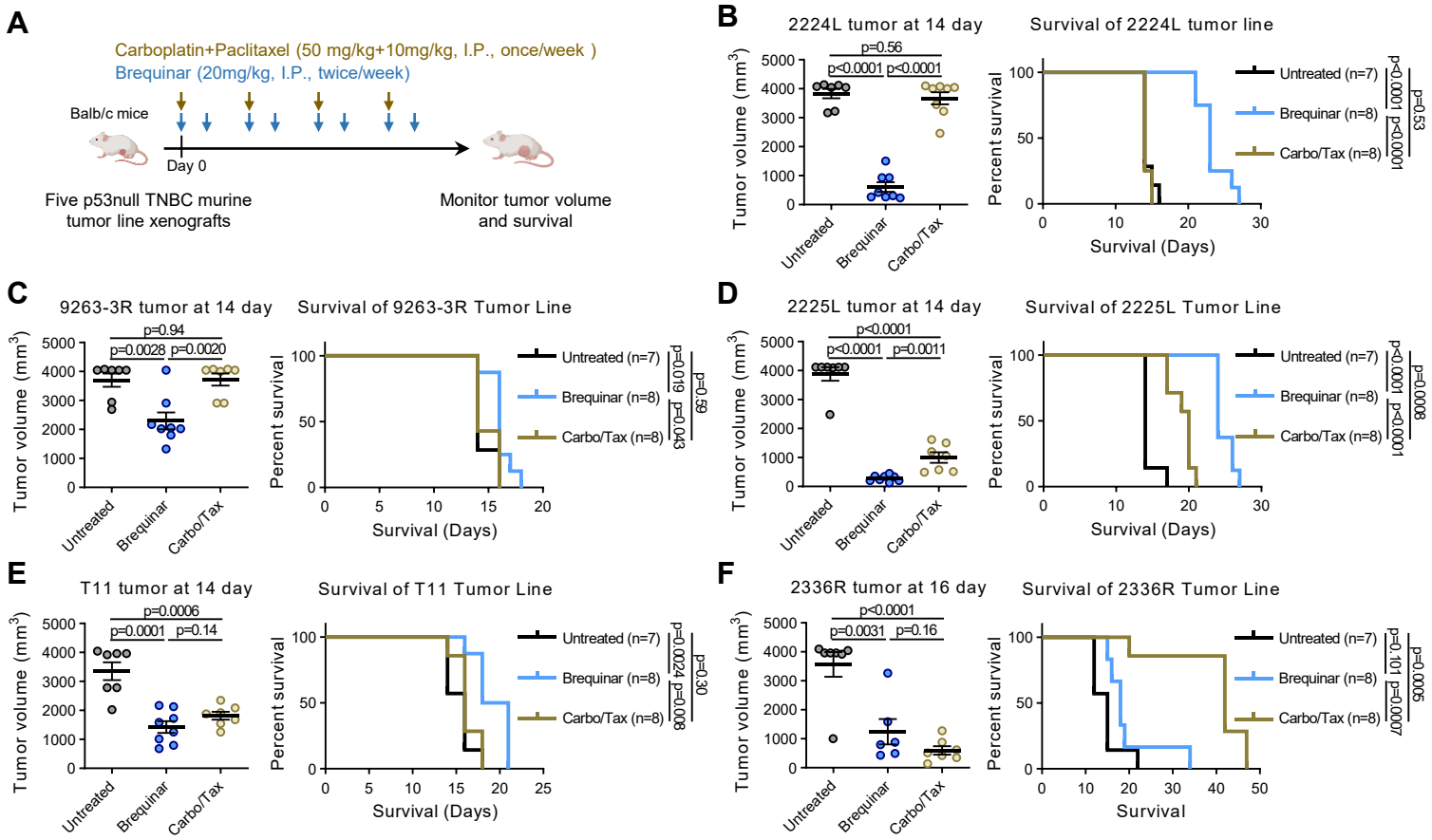

Downloaded from cancerres.aacrjournals.org on December 16, 2021. © 2021 American Association for Cancer Research.

Author Manuscript Published OnlineFirst on December 15, 2021; DOI: 10.1158/0008-5472.CAN-21-2745
Author manuscripts have been peer reviewed and accepted for publication but have not yet been edited.

Cancer Research
The Journal of Cancer Research (1916–1930) | The American Journal of Cancer (1931–1940)

AACR American Association for Cancer Research

Integrated Metabolic Profiling and Transcriptional Analysis Reveals Therapeutic Modalities for Targeting Rapidly Proliferating Breast Cancers

Chengheng Liao, Cherise Ryan Glodowski, Cheng Fan, et al.

Cancer Res Published OnlineFirst December 15, 2021.

Updated version	Access the most recent version of this article at: doi:10.1158/0008-5472.CAN-21-2745
Supplementary Material	Access the most recent supplemental material at: http://cancerres.aacrjournals.org/content/suppl/2021/12/15/0008-5472.CAN-21-2745.DC1
Author Manuscript	Author manuscripts have been peer reviewed and accepted for publication but have not yet been edited.

E-mail alerts	Sign up to receive free email-alerts related to this article or journal.
Reprints and Subscriptions	To order reprints of this article or to subscribe to the journal, contact the AACR Publications Department at pubs@aacr.org.
Permissions	To request permission to re-use all or part of this article, use this link http://cancerres.aacrjournals.org/content/early/2021/12/14/0008-5472.CAN-21-2745. Click on "Request Permissions" which will take you to the Copyright Clearance Center's (CCC) Rightslink site.

Downloaded from cancerres.aacrjournals.org on December 16, 2021. © 2021 American Association for Cancer Research.